NASA Technical Memorandum 78449

Laser-Velocimeter Surveys of Merging Vortices in a Wind Tunnel - Complete Data and Analysis

Victor R. Corsiglia, James D. Iversen,
and Kenneth L. Orloff

OCTOBER 1978

NASA

NASA Technical Memorandum 78449

Laser-Velocimeter Surveys of Merging Vortices in a Wind Tunnel - Complete Data and Analysis

Victor R. Corsiglia
Ames Research Center, Moffett Field, California
James D. Iversen
Iowa State University, Ames, Iowa
Kenneth L. Orloff
Ames Research Center, Moffett Field, California

NASA
National Aeronautics
and Space Administration

Scientific and Technical Information Office

1978

SYMBOLS

b	wing span
$\bar{r}$	radius of vortex normalized by b
U_∞	free-stream velocity
$\bar{v}$	lateral velocity normalized by U_∞ (fig. 1)
$\bar{V}$	crossflow velocity magnitude normalized by U_∞, $\bar{V} = [\bar{v}^2 + w^2]^{1/2}$
$\bar{v}_B, \bar{v}_G$	velocity values measured on the blue and green channels of the velocimeter, respectively, normalized by U_∞
$\bar{V}_C$	circumferential velocity component normalized by U_∞
$\bar{w}$	vertical velocity normalized by U_∞ (fig. 1)
$\bar{x}_w, \bar{x}_m$	streamwise distance from wing and merger point, respectively, normalized by b
$\bar{y}, \bar{z}$	coordinates from vortex center (fig. 1) normalized by b, using the vortex center obrained by flow visualization
Γ	circulation, positive counterclockwise
$\bar{\Gamma}$	$\frac{\Gamma}{bU_\infty}$
ψ	stream function
$\bar{\psi}$	$\frac{\psi}{bU_\infty}$
ζ	vorticity, positive counterclockwise
$\bar{\zeta}$	$\frac{b\zeta}{U_\infty}$

LASER-VELOCIMETER SURVEYS OF MERGING VORTICES IN A WIND TUNNEL — COMPLETE DATA AND ANALYSIS

Victor R. Corsiglia, James D. Iversen,* and Kenneth L. Orloff

Ames Research Center

SUMMARY

The merger of two corotating vortices was studied with a laser velocimeter designed to measure the two cross-stream components of velocity. Measurements were made at several downstream distances in the vortex wake shed by two semispan wings mounted on the wind-tunnel walls. The velocity data provided well-defined contours of crossflow velocity, stream function, and vorticity for a variety of test conditions. Downstream of the merger point, the vorticity was found to be independent of the downstream distance for radii smaller than $r/b = 0.05$. For larger radii, the vorticity depended on the distance from the wing. Upstream of the merger point, a multicell vorticity pattern was found.

INTRODUCTION

In recent years, considerable research into means of deintensifying the wake of large aircraft has taken place (ref. 1). Some of this work has focused on the process whereby corotational vortices merge as a technique for diffusing the wake vorticity. Experiments in this area have shown (refs. 2-4) that when the trailing-edge flaps of a large transport aircraft were set so as to shed multiple vortices per side, the vortices can merge to form a diffuse wake so that reduced rolling moments are imposed on a following aircraft. Rossow further has found (ref. 5) that a fin mounted on a wing upper surface so as to introduce an additional vortex per side into the wake also results in a greatly diffused wake. In addition, his scheme allows the wing trailing-edge flaps to be set at their usual landing position.

Several methods have been used to investigate the merger process theoretically. The point vortex interaction approach provides simplicity and contains the essential ingredients of convection. Rossow (refs. 6, 7) and Christiansen (refs. 8-10) have used this inviscid approach to show that a boundary exists between merger and nonmerger, depending on the relative strength, size, and separation of the two vortices. Another method, second-order closure theory for turbulence, provides a greater sophistication in the modeling at the expense of increased computational complexity. Using such a code, Bilanin (refs. 11 and 12) has shown that maximum turbulent kinetic energy is higher an and maximum vorticity is lower during the merging of vortices than during the decay of a single isolated vortex. He noted that the presence of two vortices destroys the axial symmetry and allows turbulence to be produced.

*Professor, Iowa State University, Ames, IA.

An intermediate technique is that of Steger and Kutler (ref. 13) wherein diffusion is included by use of a simplified viscosity model.

A need exists for detailed data describing the merger process in order to assess the relative merits of the various computational schemes. In one set of experiments directed at this need, merger was studied by flow visualization (refs. 14-16) using the same wind tunnel and models as were used in the present study. Two semispan wings mounted on the wind-tunnel walls provided two vortices whose interaction and merger were observed. The distance from the wings to the merger point correlated well with the initial vortex spacing, suitably normalized by a vortex shape parameter termed the circulation defect diameter. No boundary between merger and nonmerger was found, suggesting a significant influence of turbulent diffusion. However, the experimental data did not greatly exceed the critical spacing predicted by Rossow (ref. 6) and Christiansen (refs. 8-10).

The objective of the present study is to provide additional experimental data for various vortex merger processes in order to compare and evaluate the theoretical models described above. Time-averaged velocities were measured using a laser velocimeter on crossflow planes at several distances downstream from the wings. As a first step in the evaluation of the theories, a companion paper (ref. 17) uses the intermediate technique of Steger and Kutler (ref. 13) to calculate results for comparison with the present data. Additional results of the present study are contained in references 18 and 19.

The assistance of Professor P. Raj and student R. Brickman in recording the measurements and reducing the data is gratefully acknowledged.

WIND-TUNNEL FACILITY AND LASER VELOCIMETER

The data presented herein were obtained with a laser velocimeter installed at the Iowa State University 76- by 91-cm (30- by 36-in.) Open Circuit Wind Tunnel. This tunnel incorporates an extended test section length of 6 m in which the turbulence intensity was measured 0.1% over most of the test section with some local regions as high as 0.9%. The flow fields of interest were generated by two semispan wings mounted on the bottom and side walls of the test section at any one of four streamwise locations (fig. 1). These wings were identical NACA 0012 airfoils with constant chord and elliptical tips. The distance that each wing protruded into the test section was adjustable so that the relative position of the shed vorticity could be varied. The installation of the wings was identical to that of earlier studies (refs. 14, 15) and additional details are contained there.

The laser velocimeter, shown schematically and photographically in figure 2, was especially designed for the present experiment. It incorporated two dual-scatter crossed-beam systems that operated independently at wavelengths of 488.0 (blue) and 514.5 (green) nanometers originating from a single

argon-ion laser. This instrument differed from an earlier version of the two-color laser velocimeter (ref. 19) only in the arrangement of the optical components, the use of fixed focal length optics rather than scanning optics, and the use of acousto-optic cells in each channel to eliminate directional ambiguity. Inclining the green output channel at 30° to the blue in the vertical plane arranged the optical components so as to make the velocimeter sensitive to the two crossflow components of velocity.

The lateral v and vertical w components of velocity were obtained by the following combination of the velocities measured by the blue and green channels of the velocimeter.

$$v = -2[v_G \cos \theta - v_B \cos(30 - \theta)]$$

$$w = 2[v_G \sin \theta + v_B \sin(30 - \theta)]$$

where θ in the inclination of the centerline of the blue optics channel ($\theta = 10°$). The streamwise velocity u was measured by rotating either beam-splitter by 90° to align the plane of the output beams in the x-direction.

The amplified outputs of the photomultiplier (PM) tubes (fig. 3) were analyzed with a two-channel frequency tracker described elsewhere (ref. 20). The tracker was used to demodulate the velocimeter signals, thus providing voltages proportional to the PM tube signal frequencies. The voltages were then passed to an analog scaling computer that was used to resolve the above equations into the w and v velocity components.

Using the method described in reference 21, the spatial resolution of the optical system was estimated by computing the probe volume size and accounting for the off-axis receiving optics. The dimensions of this sensing volume were computed to be $0.3 \times 0.3 \times 1.8$ mm. Accuracy of the mean velocity measured within this probe volume was determined from the frequency tracker and analog scaler specifications to be within 2% for the v and w components of velocity.

Vertical translation of the probe volume was accomplished by raising and lowering the entire velocimeter on a hydraulic table. Lateral motion was accomplished by manual positioning of the system on rails with ball-bushing support. Positions were reproducible to within 1.0 mm.

To ensure the acquisition of nearly continuous signals, an aerosol of mineral oil was injected upstream of the wind-tunnel inlet. By strategically placing the aerosol outlet the region of interest could be adequately seeded.

PROCEDURES AND CONDITIONS

For each test, both wings were set at the same span and angle of attack ($\alpha = 10°$), and the wind-tunnel speed was set to approximately 46 m/sec (Reynolds number = 4.7×10^5 based on chord).

In earlier studies (refs. 22, 23) where the velocities in the vortices were also measured, a high-speed traverse was required to circumvent the problem of meander of the vortex center due to large-scale wind-tunnel turbulence. In the present tests, the vortex meander was greatly reduced so there was no need to rapidly scan the region of interest. Data were taken only when the vortex center was observed to be in a prescribed location. To accomplish this, the vortex was observed with the aid of a light slit and two crossing lines made up of a shadow and a laser beam (fig. 4). Data were continuously averaged to remove high-frequency noise (time constant = 0.3 sec) and sampled several times at each point. In this way, repeatability of the results was generally within 4%. Measurements were taken in 10-mm increments vertically and laterally at those locations where there was sufficient aerosol to seed the flow (20-mm grid increments for the streamwise velocity component). Up to 380 locations were measured at a streamwise location for a single configuration.

RESULTS

Figure 5 shows the locations at which data were obtained for the case of the greatest distance downstream of the merger point ($\bar{x}_m = 3.0$). Merger distance was calculated using the expression found empirically in references 14 and 15. The lateral distribution of the vertical and lateral component of velocity is also shown for two values of vertical position. The scan through the vortex center shows points missing in the center due to lack of seeding material there. Two rows away from the center, however, there was adequate seeding of the flow for the entire scan. Tunnel-wall corrections were not applied to the data because an estimate of these corrections indicated that they were small compared to the measured cross-stream velocities.

The streamwise component of velocity was measured in a separate survey from the crossflow velocity measurements because the laser velocimeter could determine only two components of velocity at a time. The streamwise velocity component is presented in figures 6 and 7 for several configurations. A variation of up to 5% was found (fig. 7). However, this variation was not attributed to the vortices, since a similar variation was found when the wings were set to zero angle of attack (fig. 6). This result is in agreement with earlier studies (refs. 22-24) wherein the streamwise component of velocity differed appreciably from free stream only over a limited radial extent from the vortex axis, and that variation was associated with loss of total head due to friction on the wing. In the present study, small values of radius could not be attained, and negligible total head loss was expected since the wings were thin and smooth.

The crossflow velocity magnitude was computed according to the expression.

$$\bar{V} = (\bar{v}^2 + \bar{w}^2)^{1/2}$$

These results were plotted in both the vertical and lateral directions, and contours of constant values of $\bar{V}$ were obtained (fig. 8). The symbols on

the figure indicate the points available from cross-plot. As can be seen, the contours are well defined over much of the region and vortex merger seems complete.

The stream function shown on the lower part of the figure was computed as follows. For two-dimensional flow in the y-z plane, the stream function is defined as

$$\psi_2 - \psi_1 = \int_1^2 -v\, dz + w\, dy \tag{1}$$

The integration was accomplished by fitting four consecutive velocity points in the y or z direction with a third-order Lagrange polynomial and interpolating for a Gauss-Legendre quadrature. The integral would be exact if the velocity distribution were a polynomial of degree 3 or less. Also, if the flow were not two-dimensional, equation (1) would lead to some error since, from Stokes theorem and continuity, the closed contour line integral of equation (1) is

$$\oint -v\, dz + w\, dy = \iint \frac{\partial u}{\partial x}\, dy\, dz \tag{2}$$

If the streamwise velocity is independent of x, equation (2) is identically zero. This calculation was performed for each 10-mm square for which velocity data were obtained. The values for the contour line integral calculated in this way were not only small but also random in sign. The flow was thus assumed to be sufficiently two-dimensional that the stream-surface cross sections calculated by equation (1) were independent of the path used.

To calculate the stream function at any one point in the flow field, a reference point was selected at which the value of the stream function was arbitrarily set equal to zero. The stream function at every point in the flow field was then obtained by calculating the change in stream function according to equation (1) along the combination of lateral and vertical distance increments Δv and Δz which provided the shortest integration length. This has the effect of minimizing the error due to axial velocity gradient (eq. (2)). As can be seen, very smooth, nearly circular, stream function contours were obtained. The smoothness of the plot as compared to the $\bar{V}$ plot reflects the smoothing effect of the calculation.

Figure 8(c) shows contours of constant vorticity. To obtain these values the data were differentiated using the following four-point expression:

$$\zeta = \frac{\partial w}{\partial y} - \frac{\partial v}{\partial z}$$

$$= \frac{1}{20}\left[(w_2 - w_1 + w_3 - w_4) - (v_4 - v_1 + v_3 - v_2)\right]$$

where the subscripts refer to the four corners of a measured grid element. These results show (fig. 8(c)) a lower degree of axial symmetry in the vorticity than in the stream function or velocity. An interesting feature is the wave pattern (approximately seven periods per revolution) around the vortex. A similar feature was noticed by Mertaugh et al. (ref. 25) in their hot-wire anemometer surveys of the near-field wake of a full-scale aircraft in flight.

A calculation was made to determine the magnitude of the error that might occur in the numerical calculation of vorticity. For this purpose, an equation for the circumferential velocity was chosen that approximates the velocity values shown in figure 8:

$$\bar{V}_c = -1.22\bar{r} + 0.25 \tag{3}$$

From this expression, both vertical and lateral components of velocity were computed at a set of grid points to simulate the measured data. The vorticity was then computed numerically by use of the procedure given earlier in the paper and by use of an analytical expression derived from equation (3):

$$\zeta = \frac{\bar{V}_c}{\bar{r}} + \frac{d\bar{V}_c}{d\bar{r}}$$

These two vorticity results are compared in figure 9. As can be seen, the numerically computed values differ only slightly from the exact circular contours. It was, thus, concluded that the numerical procedure was accurate enough for the present purposes.

Figure 10 shows a set of contours of crossflow velocity, stream function, and vorticity at a streamwise location nearer to but still downstream of the merger point $\bar{x}_m = 1.2$. Although the stream function contours appear smooth and circular, the velocity and vorticity both lack axial symmetry when compared with the previous figure. In fact, a significant second cell of vorticity is present at $\bar{x}_m = 1.2$. Merger has been defined as the coalescence of vortex centers based on flow visualization. If merger were defined as the coalescence of centers of vorticity, then the vortices shown in figure 10 would not be merged.

The comparable results at a streamwise location even closer to the merger point ($\bar{x}_m = 0.8$) are presented in figure 11. To obtain data at this value of $\bar{x}_m$, the span of the wings was reduced by 3% to achieve an increase in the initial vortex spacing, and the distance from the wings to the measurement point was increased to 7.4 spans. The shapes of the velocity and stream function contours are similar to those in figure 10. The wave pattern around the vortex in the vorticity contour is still evident.

To compare the results shown in figures 8, 10, and 11 with each other, an average radius for each contour level of the vorticity was obtained. This was done by equating the area within each contour level (ignoring the secondary cells) to the area of a circle. The distribution of vorticity with average radius forms a single curve for all three configurations (fig. 12). These

results show that within $\bar{r} = 0.05$ there is no evidence of diffusion of vorticity over the range of distances tested. A Lamb vortex profile fits this curve well to a radius $\bar{r} = 0.02$: this profile does not strictly apply, however, because it represents the decay of a line vortex instead of the decay of two distributed vortices in proximity of one another, which is the present case.

A similar comparison can be made by computing the circulation. To obtain these values, the component of velocity which is tangent to a circle of radius $\bar{r}$ was computed according to the expression

$$\bar{V}_c = \left(\frac{\bar{w}\bar{y} - \bar{v}\bar{z}}{\bar{y}^2 + \bar{z}^2} \right)^{1/2}$$

The area within contours of circumferential velocity (not shown) was then measured to obtain the average radius from which the circulation was computed as follows:

$$\bar{\Gamma} = 2\pi \bar{r} \bar{V}_c$$

The results show (fig. 13(a)) that, to a radius $\bar{r} = 0.05$, the circulation profiles are also nearly identical. This agrees with the result shown on the previous figure. However, at larger radii there is evidence of outward diffusion or convection of vorticity as seen by the lower circulation values. The results for $\bar{x}_w = 7.2$ and 7.4 nearly superimpose and are lower than the results for $\bar{x}_w = 5.8$. On the other hand, the distances from the merger point are not in the same order as the circulation curves. It can be concluded that the vortex decay process depends primarily on the distance from the wings.

For comparison, the circulation profiles for a single wing are shown (fig. 13(b)). The circulation rises slightly with downstream distance indicating that the rollup process is still occurring. Also shown is a calculated profile using the method of Betz as discussed by Rossow (ref. 26). The Betz profile agrees with the measured profile for the maximum downstream distance $\bar{x}_w = 7.2$. Since no decrease in circulation with increasing downstream distance was found for the single-wing case (in contrast with the decrease found for the two-wing case), the vortex decay shown in figure 13(a) must be the result of the presence of the second vortex.

Figure 14 shows the results at a streamwise location upstream of the merger point $\bar{x}_m = -4.2$. The separation of the two vortices is clear and agrees with the location obtained by flow visualization. The crossflow velocity vanishes in the region midway between the vortex centers as would be expected. An interesting feature of the data presented in figure 14(c) is the multicell pattern of the vorticity contours, possibly caused by incomplete rollup of the vorticity from each wing, since the single wing results showed incomplete rollup at $\bar{x}_w = 3.0$ (fig. 13) compared to $\bar{x}_w = 1.8$ in figure 14. Since the distance between the main vortices in the pattern is comparable to the distance between the small vortices and their nearest neighbor, the merger process and the initial rollup process appear to be occurring simultaneously.

ADDITIONAL CONFIGURATIONS

Contours of velocity, magnitude, and vorticity for those configurations in table 1 not presented earlier are contained in figures 15-17.

CONCLUSIONS

Detailed surveys were performed of the velocity field of two vortices undergoing a merger process. Sufficient velocity data were obtained to define the crossflow stream function and vorticity over a plane at several streamwise locations both upstream and downstream from the merger point. The axial symmetry of the merged vortex decreased as the merger point was approached from downstream with secondary cells evident at the nearer locations. Downstream of the merger point within a small radius from the vortex center, the vorticity was shown to be independent of streamwise location. At larger radii, the reduction in vorticity with downstream distance was found to depend on the distance from the wing rather than the distance from the merger point. A single isolated vortex showed no aging over the streamwise distances studied. It was therefore concluded that the second vortex was responsible for the reduction in vorticity. At a streamwise location forward of the merger point, a multicell vorticity pattern was found.

Ames Research Center
National Aeronautics and Space Administration
Moffett Field, Calif. 94035, June 21, 1978

REFERENCES

1. Hallock, J. N.: Aircraft Wake Vortices: An Annotated Bibliography (1923-1975), Transportation Systems Center, Cambridge, Mass. FAA-RD-76-43, Jan. 1976.

2. Corsiglia, Victor R.; Rossow, Vernon J.; and Ciffone, D. L.: Experimental Study of the Effect of Span Loading on Aircraft Wakes. J. Aircraft, vol. 13, no. 12, Dec. 1976, pp. 968-973.

3. Ciffone, Donald L.: Vortex Interactions in Multiple Vortex Wakes Behind Aircraft. J. Aircraft, vol. 14, no. 5, May 1977, pp. 440-446.

4. Corsiglia, Victor R.; and Dunham, R. Earl, Jr.: Aircraft Wake-Vortex Minimization by Use of Flaps. Proceedings, NASA Symposium on Wake Vortex Minimization, Washington, D.C., Feb. 25-26, 1976, pp. 305-338 (NASA SP-409).

5. Rossow, V. J.: Effect of Wing Fins on Lift-Generated Wakes. AIAA Paper 77-671, AIAA 10th Fluid & Plasma Dynamics Conference, Albuquerque, New Mexico, June 27-29, 1977.

6. Rossow, Vernon J.: Convective Merging of Vortex Cores in Lift-Generated Wakes. J. Aircraft, vol. 14, no. 3, March 1977, pp. 283-290.

7. Rossow, Vernon J.: Inviscid Modeling of Aircraft Trailing Vortices. Proceedings, NASA Symposium on Wake Vortex Minimization, Washington, D.C., Feb. 25-26, 1976, pp. 9-59 (NASA SP-409).

8. Roberts, K. V.; and Christiansen, J. P.: Topics in Computational Fluid Mechanics. Computer Physics Communications, Suppl., vol. 3, 1972, pp. 14-32.

9. Christiansen, J. P.: Numerical Simulation of Hydrodynamics by the Method of Point Vortices. J. Comput. Phys., vol. 13, 1973, pp. 363-379.

10. Christiansen, J. P.; and Zabuski, N. J.: Instability, Coalescence and Fission of Finite-Area Vortex Structures. J. Fluid Mech., vol. 61, pt. 2, 1973, pp. 219-243.

11. Bilanin, Alan J.; Teske, Milton E.; Donaldson, Coleman; and Snedeker, R. S.: Viscous Effects in Aircraft Trailing Vortices. NASA Symposium on Wake Vortex Minimization, Washington, D.C., 1976, pp. 61-128, (NASA SP-409).

12. Bilanin, Alan J.; Teske, Milton E.; and Williamson, G. G.: Vortex Interactions and Decay in Aircraft Wakes. AIAA J., vol. 15, no. 2, Feb. 1977, pp. 250-260.

13. Steger, Joseph L.; and Kutler, Paul: Implicit Finite-Difference Procedure for the Computation of Vortex Wakes. AIAA J., vol. 15, no. 4, April 1977, pp. 581-590.

14. Brandt, S. A.: Interaction and Merging of Aircraft Trailing Vortices. Master of Science Thesis, Iowa State University, Ames, Iowa, 1976.

15. Brandt, S. A.; and Iversen, J. D.: Merging of Aircraft Trailing Vortices. Paper 77-8, AIAA 15th Aerospace Sciences Meeting, Los Angeles, Calif., Jan. 24-26, 1977.

16. Iversen, J. D.; Brandt, S. A.; and Raj, P.: Merging Distance Criteria for Co-rotating Trailing Vortices. Conference on Aircraft Wake Vortices, Cambridge, Mass., March 15-17, 1977. Rept. FAA-RD 77-68.

17. Raj P.; and Iversen, J. D.: Computational Studies of Turbulent Merger of Corotational Vortices. AIAA Paper 78-108, AIAA 16th Aerospace Sciences Meeting, Huntsville, Ala., Jan. 16-18, 1978.

18. Iversen, J. D.; and Corsiglia, V. R.: The Role of Turbulence in Vortex Wake Decay. Iowa State University Report ERI 77393, June 1977.

19. Grant, George R.; and Orloff, Kenneth L.: Two-Color Dual-Beam Back-scatter Laser Doppler Velocimeter. Appl. Opt., vol. 12, no. 12, Dec. 1973, pp. 2913-2916.

20. Orloff, K. L.; Corsiglia, V. R.; Biggers, J. C.; and Ekstedt, T. W.: Investigating Complex Aerodynamic Flows with a Laser Velocimeter, the Accuracy of Flow Measurements by Laser Doppler Methods. Proceedings of the LDA-Symposium, Copenhagen, Denmark, Aug. 25-28, 1975, pp. 624-643. (Also NASA TM X-73,171.)

21. Goethert, W. H.: Laser Doppler Velocimeter Dual Scatter Probe Volume. AEDC-TR-71-85, July 1971.

22. Corsiglia, V. R.; Schwind, R. G.; and Chigier, N. A.: Rapid Scanning, Three-Dimensional Hot-Wire Anemometer Surveys of Wing-Tip Vortices. J. Aircraft, vol. 10, no. 12, Dec. 1973, pp. 752-757.

23. Corsiglia, V. R.; and Orloff, K.: Scanning Laser-Velocimeter Surveys and Analysis of Multiple Wakes of an Aircraft. Conference on Aircraft Wake Vortices, Cambridge, Mass., Rept. FAA-RO 77-68, March 15-17, 1977. (Also NASA TM X-73,168, 1976.)

24. Orloff, Kenneth L.: Trailing Vortex Wind-Tunnel Diagnostics with a Laser Velocimeter. J. Aircraft, vol. 11, no. 8, Aug. 1974, pp. 477-482.

25. Mertaugh, Lawrence J.; Damania, Rustom B.; and Paillet, F. L.: An Investigation of the Near-Field Wake behind a Full-Scale Test Aircraft. J. Aircraft, vol. 14, no. 9, Sept. 1977, pp. 894-902.

26. Rossow, Vernon J.: On the Inviscid Rolled-Up Structure of Lift Generated Vortices. J. Aircraft, vol. 10, no. 11, Nov. 1973, pp. 647-650.

TABLE 1.- LIST OF CONFIGURATIONS

b, c_m	$\bar{x}_w$	$\bar{x}_m$	Merged	Figure
Two wings, $\alpha = 10°$				
66	8.2	-5.4	No	15(d)-(f)
72.4	7.4	0.8	Yes	11
72.4	3.3	-4.1	No	15(a)-(c)
72.4	1.8	-4.2	No	14
74.9	7.2	3.0	Yes	8
74.9	5.8	1.2	Yes	10
Two wings, $\alpha = 8°, 12°$				
72.4	7.4	--	Yes	16(a)-(c)
	3.3	--	No	16(d)-(f)
Single wing, $\alpha = 10°$				
74.9	7.2	--	--	17, 13
	5.8	--	--	13
	3.2	--	--	13

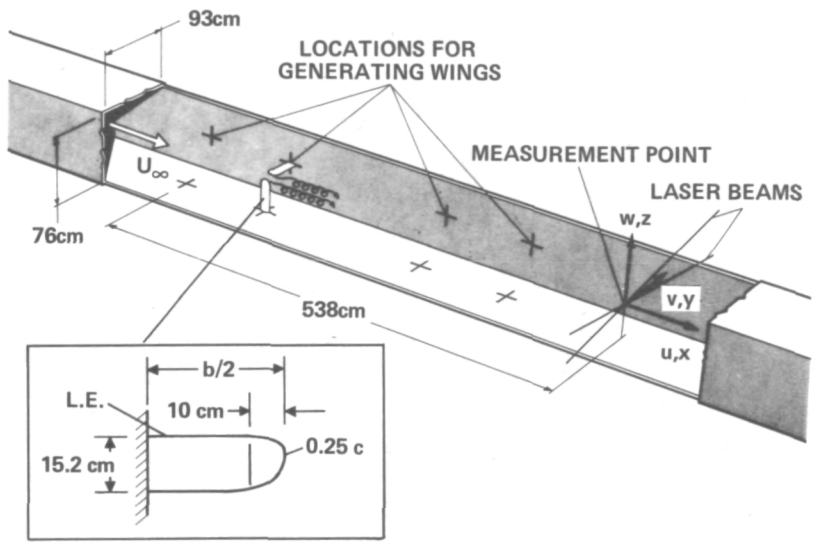

(a) Schematic.

Figure 1.- Test installation.

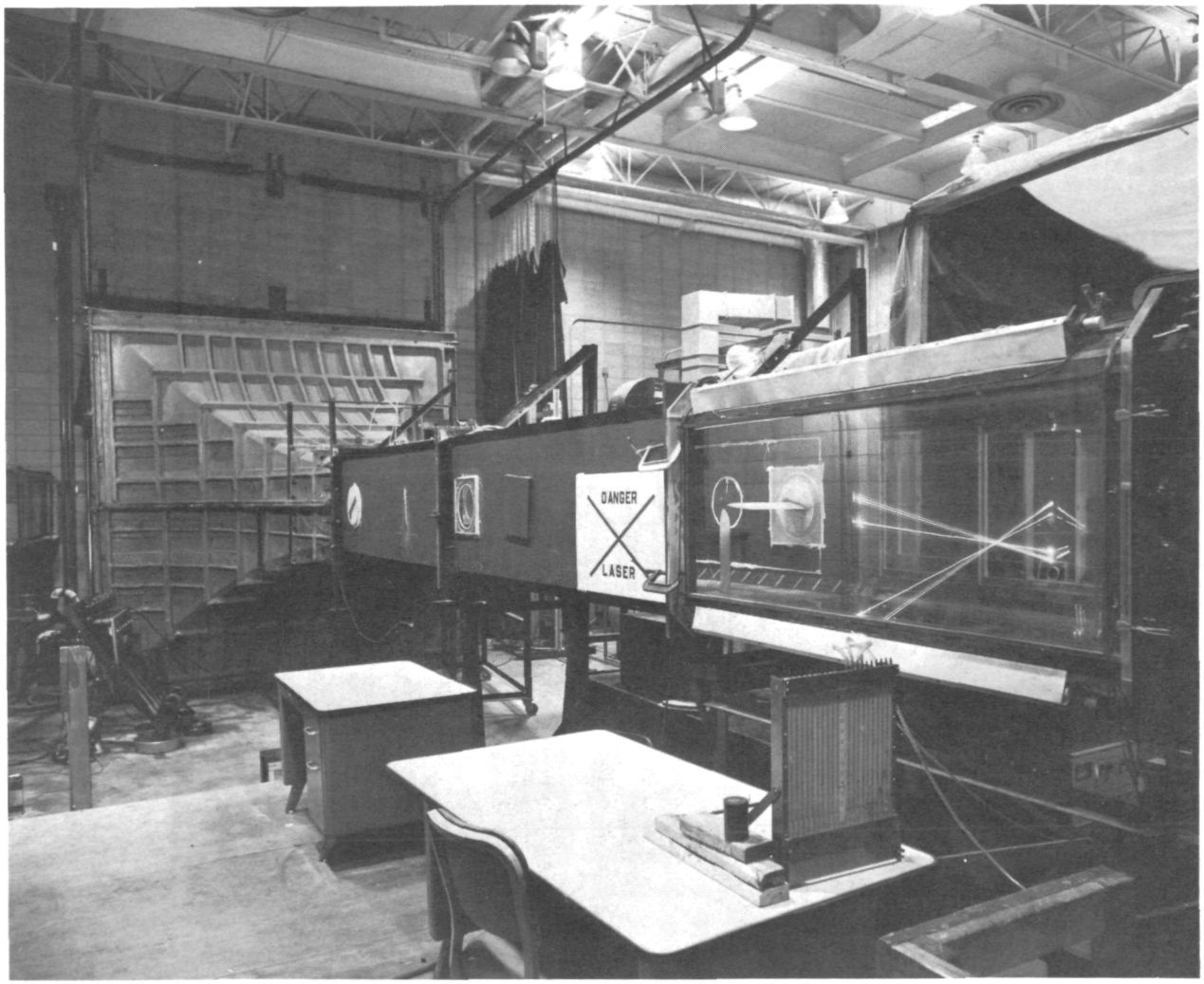

(b) Photograph.

Figure 1.- Concluded.

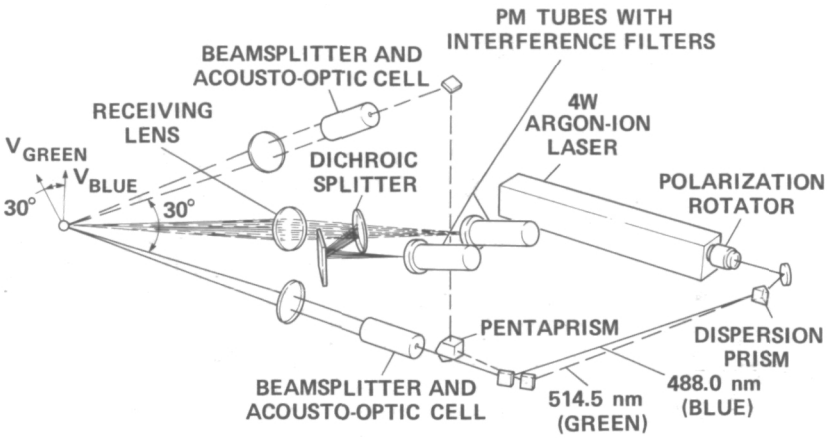

(a) Schematic of optical arrangement.

Figure 2.- Laser velocimeter.

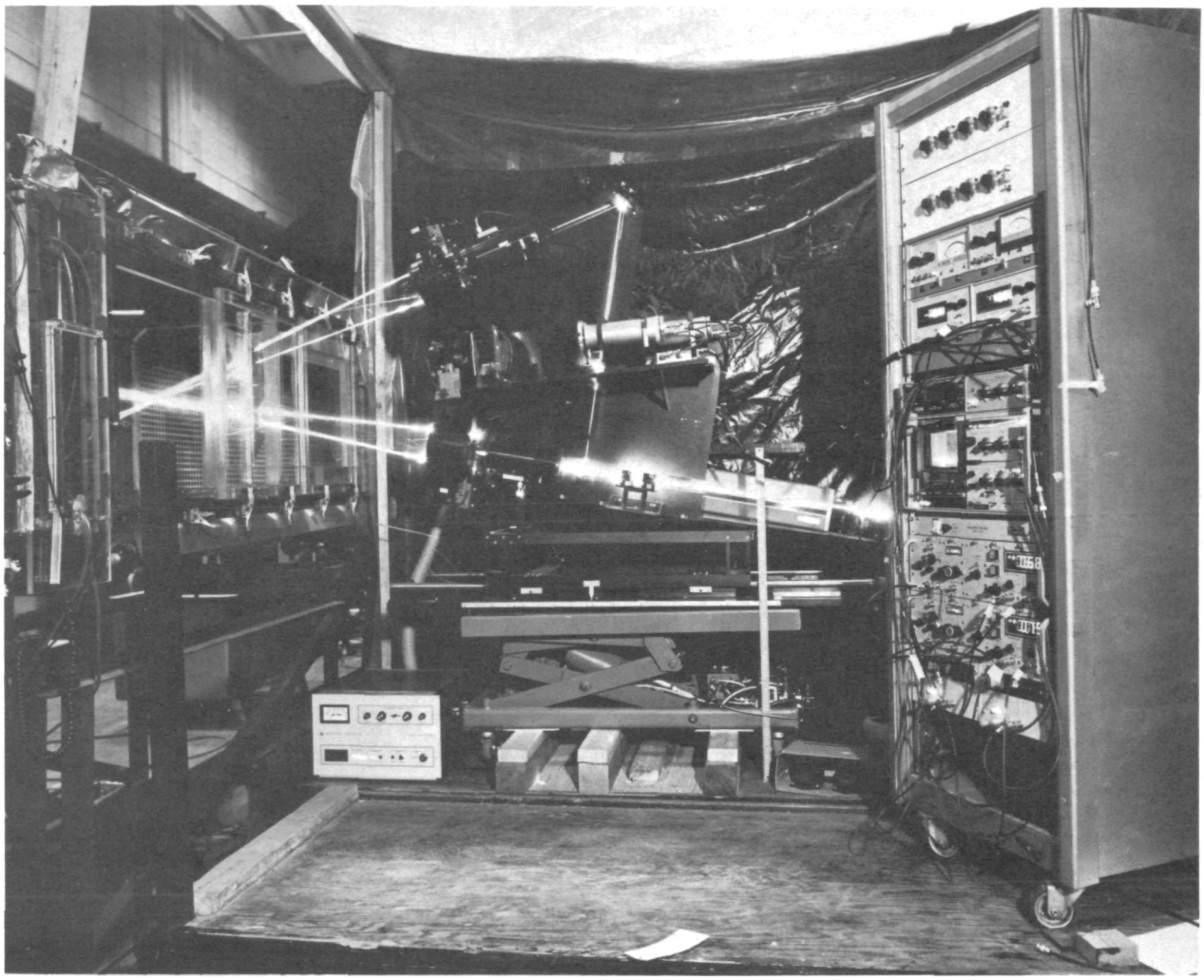

(b) Photograph of laser velocimeter installation.

Figure 2.- Concluded.

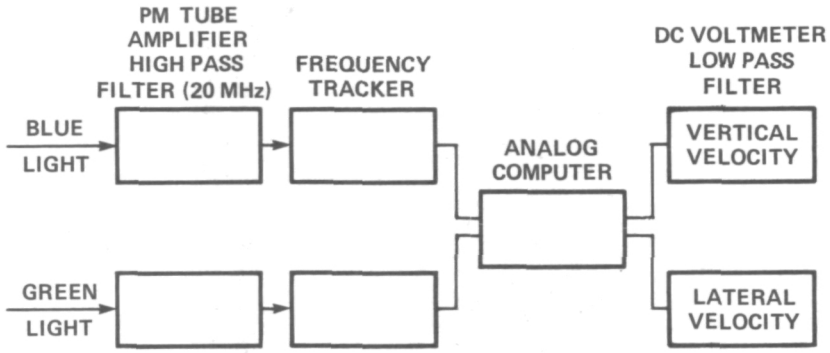

Figure 3.- Schematic of the electronic signal processing.

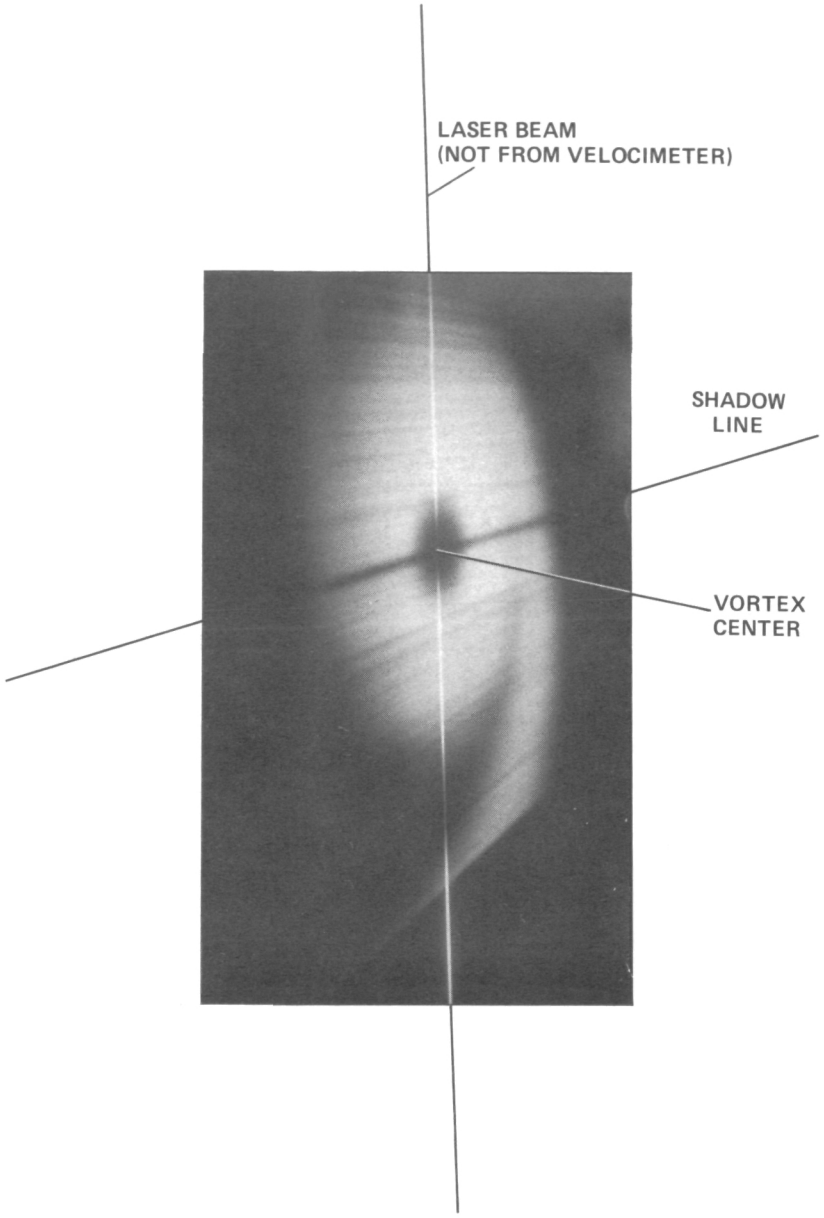

Figure 4.- Light slit photograph to illustrate flow visualization of the vortex center. The vortex center appears dark due to the absence of seeding material.

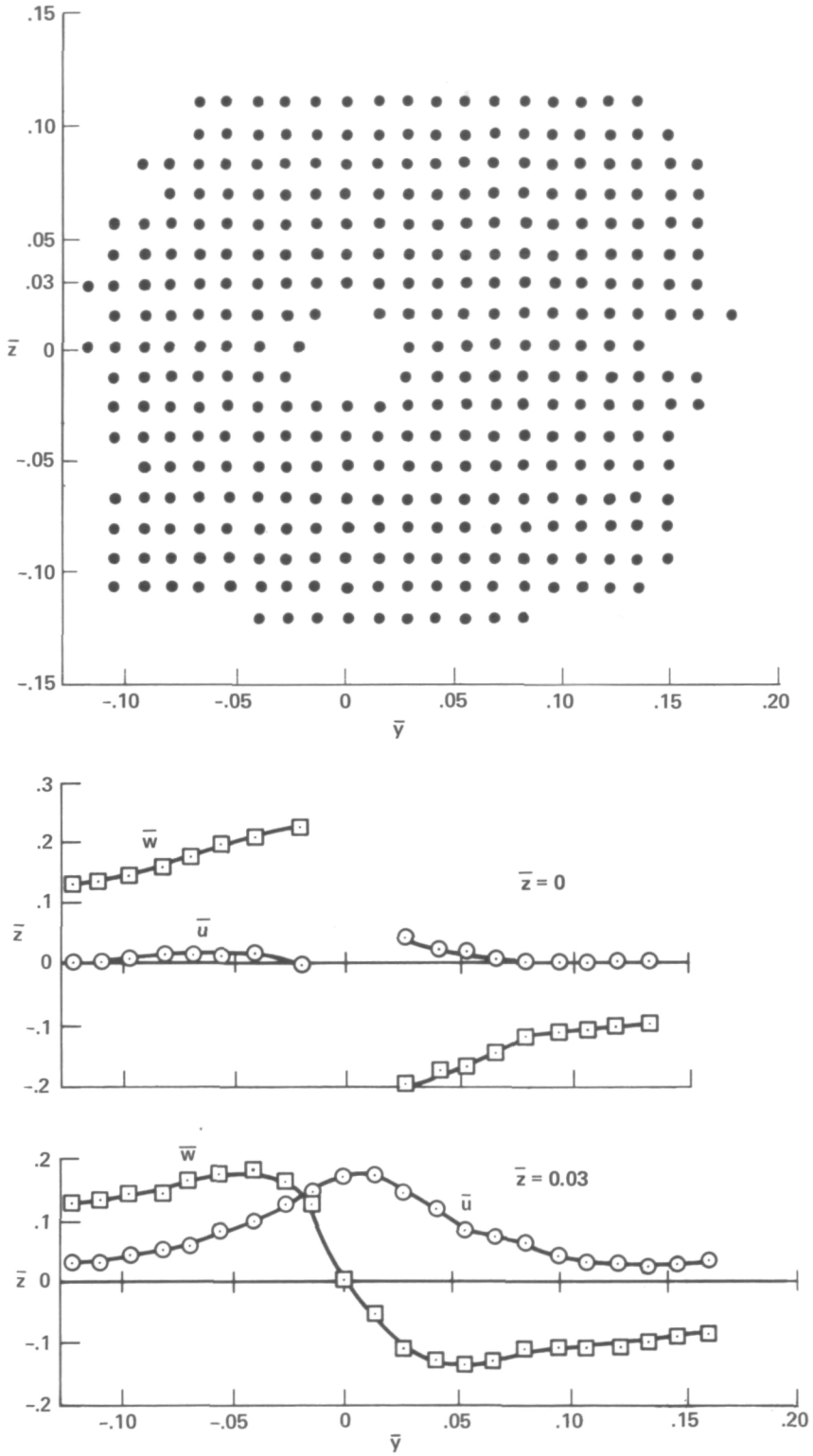

Figure 5.- Grid of data obtained and typical measured results of velocity survey; b = 749 mm, $\bar{x}_w$ = 7.2, $\bar{x}_m$ = 3.0.

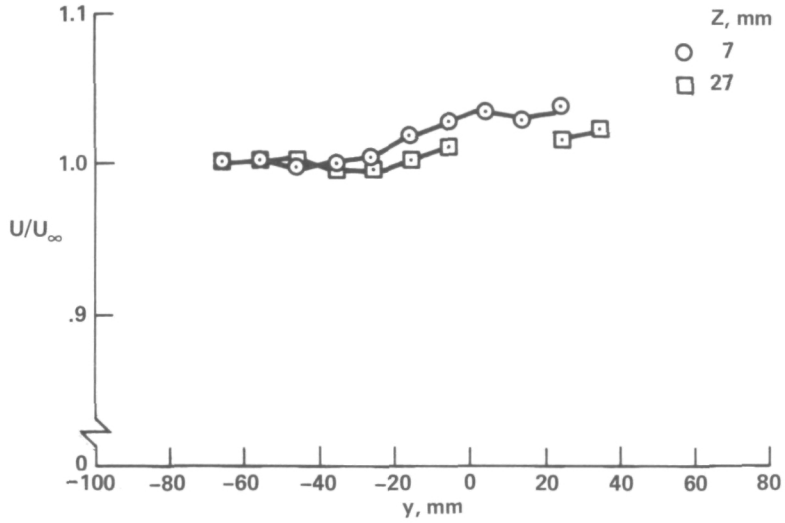

Figure 6.- Streamwise velocity component with no vortex in the wind tunnel for two horizontal traverses; y and z reference same as in figure 7(a); $\alpha = 0°$, $\bar{x}_w = 3.2$, b = 72.4 cm, 2 wings.

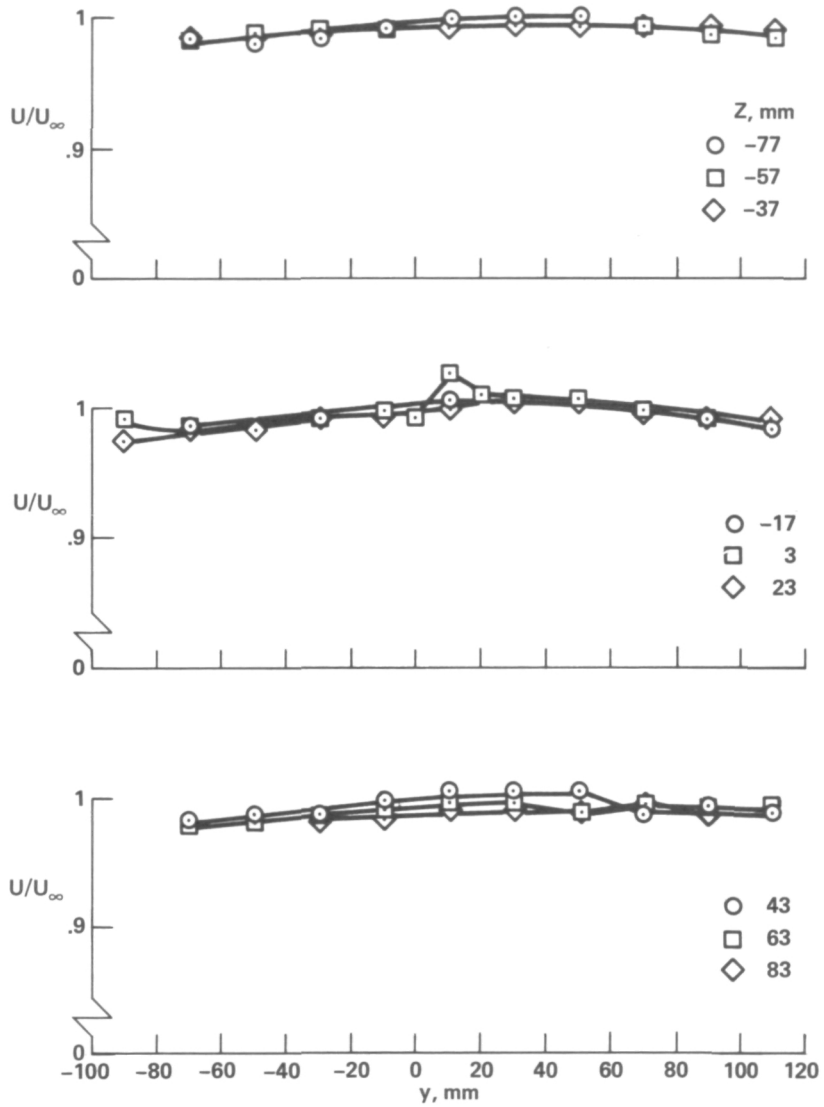

(a) $\bar{x}_w = 7.4$

Figure 7.- Streamwise velocity component with vortex in tunnel for various horizontal traverses at different distances from the vortex center; $\alpha = 10°$, b = 72.4, 2 wings.

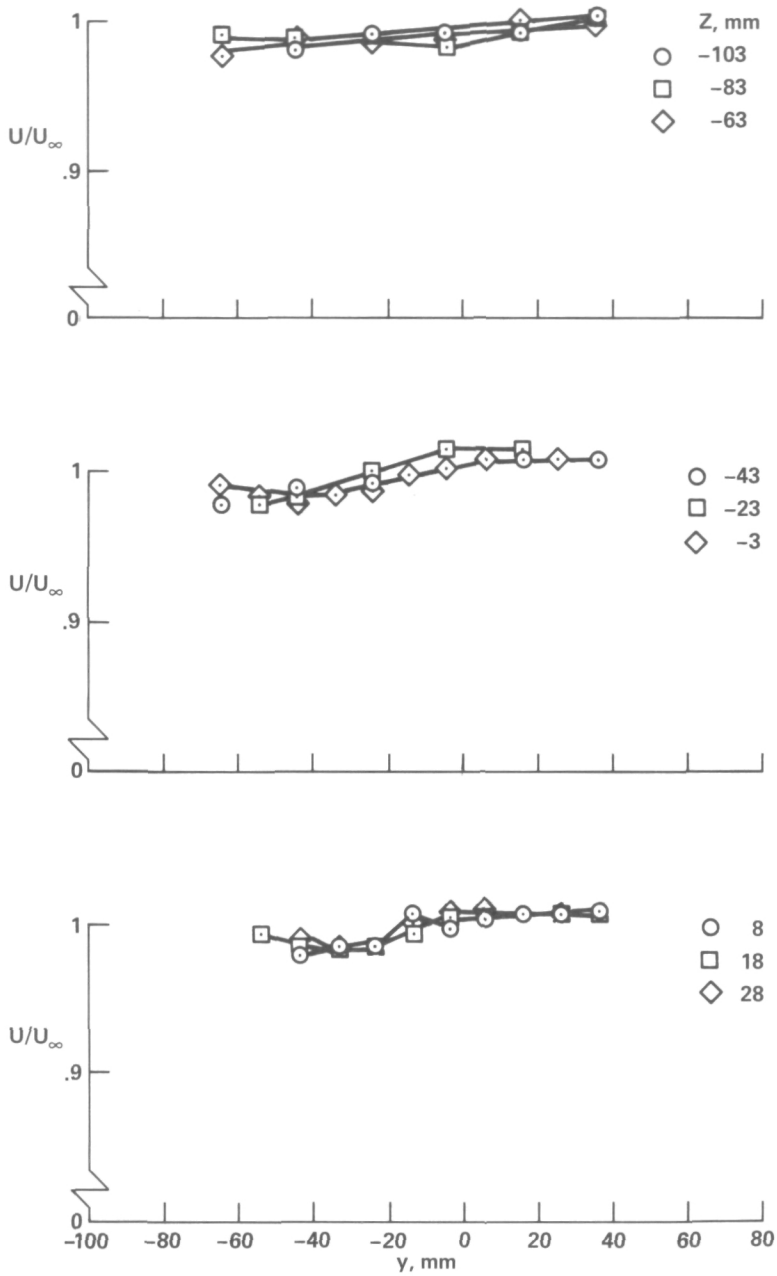

(b) $\bar{x}_w = 3.2$

Figure 7.- Continued.

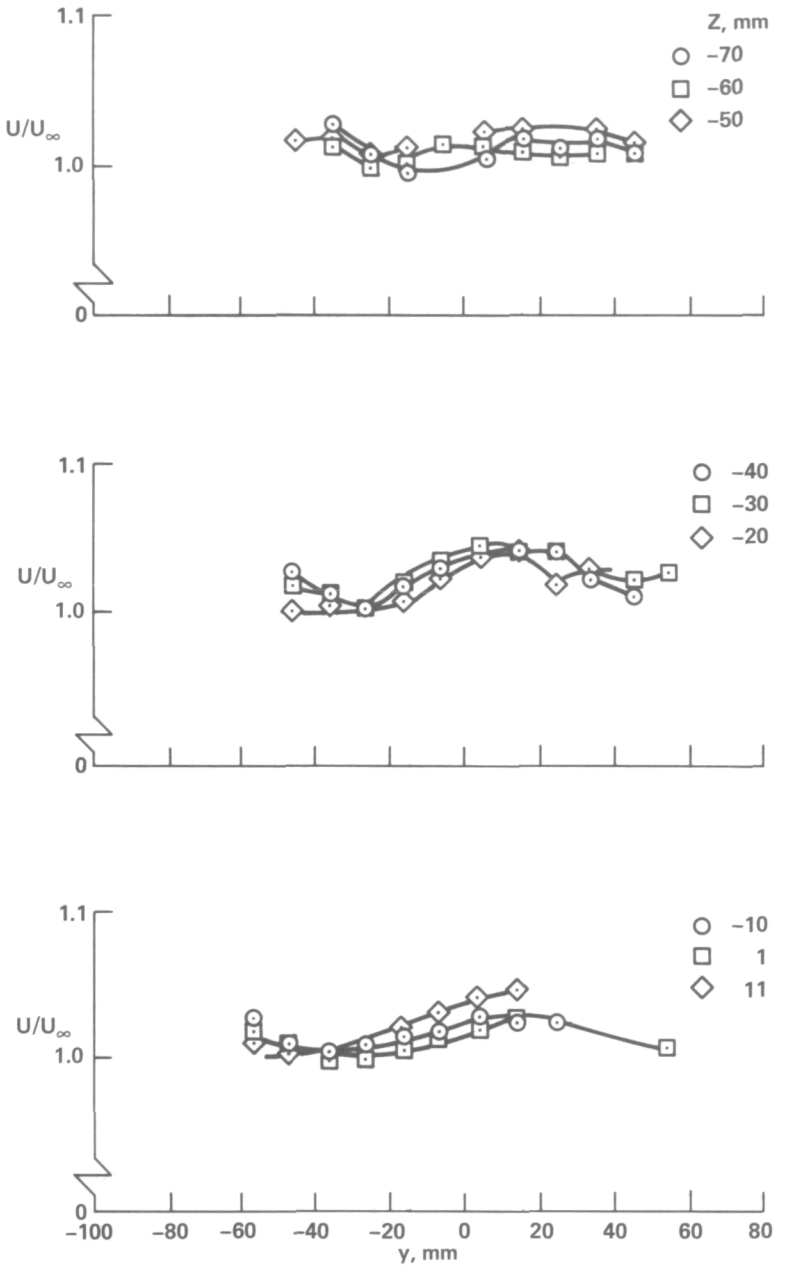

(c) $\bar{x}_w = 1.8$

Figure 7.- Concluded.

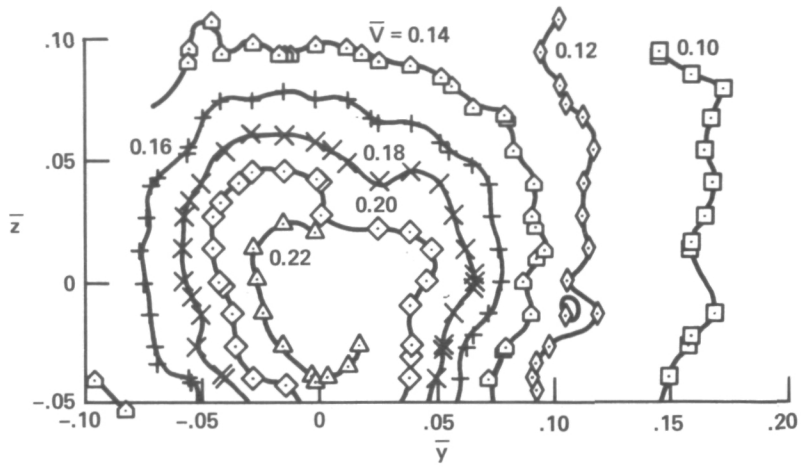

(a) Crossflow velocity.

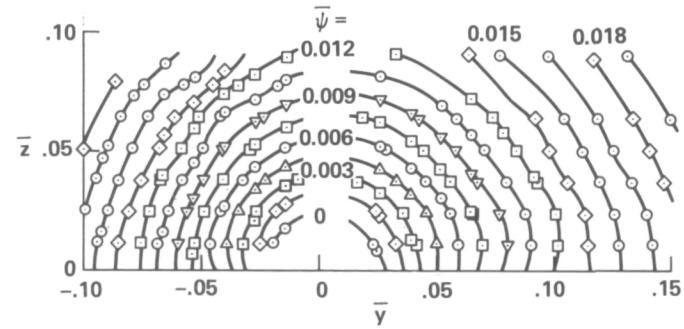

(b) Stream function.

Figure 8.- Results calculated from the measured velocities; b = 749 mm, $\bar{x}_w$ = 7.2, $\bar{x}_m$ = 3.0.

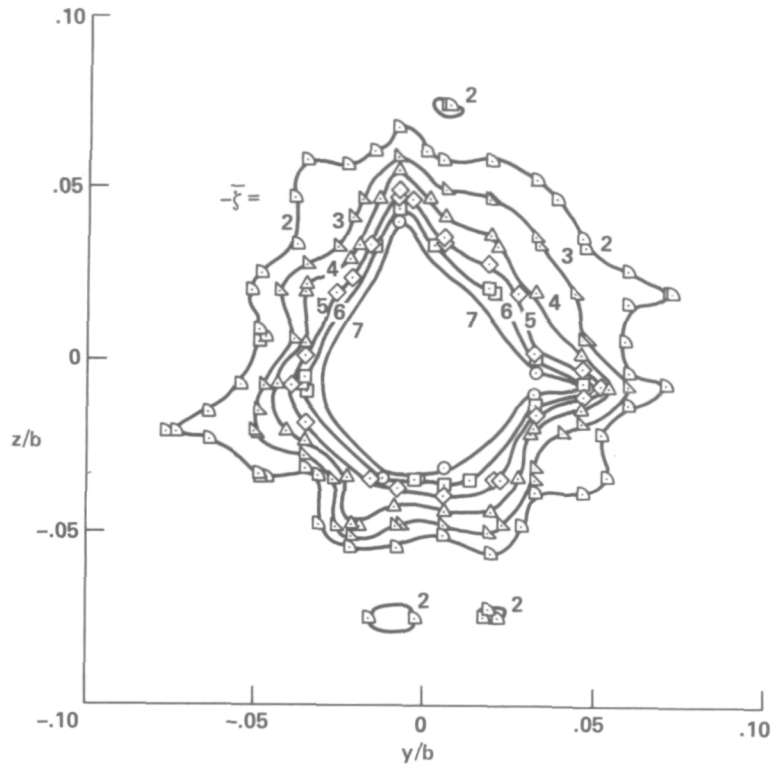

(c) Vorticity.

Figure 8.- Concluded.

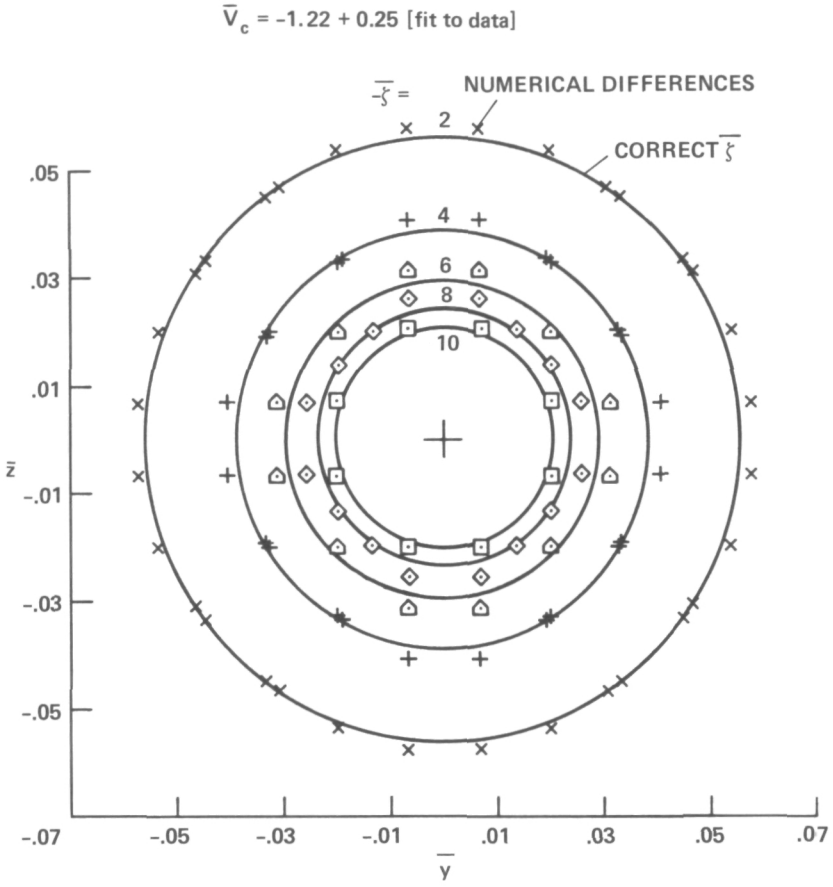

Figure 9.- Comparison of vorticity magnitudes as calculated by numerical method and by exact vorticity expression for an axisymmetric vortex that approximates the measured velocities; b = 749 mm, $\bar{x}_w$ = 7.2, $\bar{x}_m$ = 3.0.

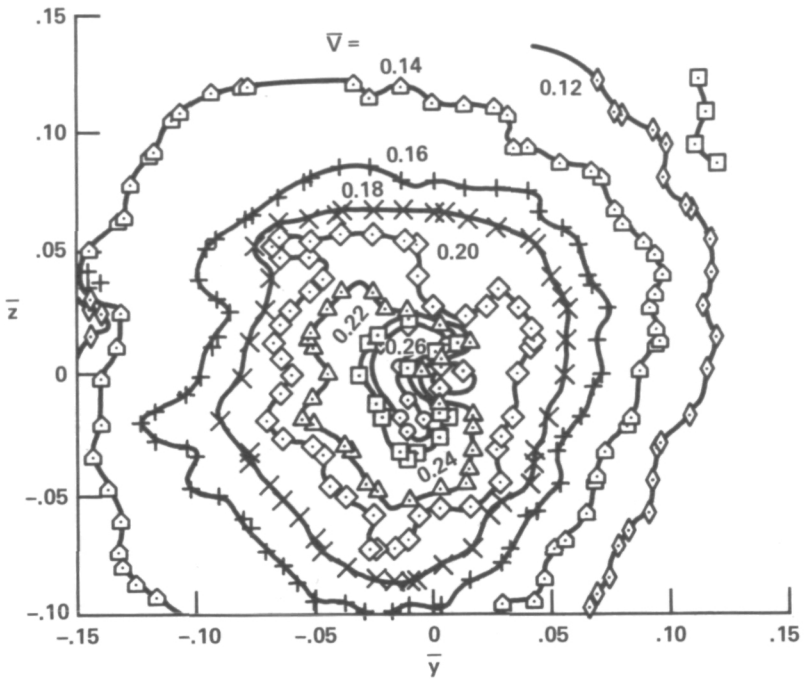

(a) Crossflow velocity.

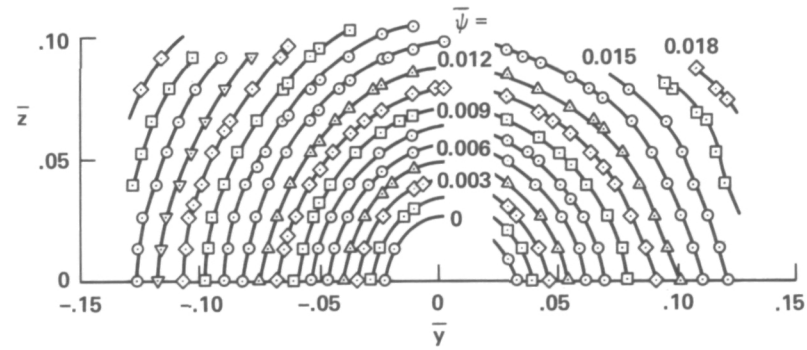

(b) Stream function.

Figure 10.- Results calculated from the measured velocities; b = 749 mm, $\bar{x}_{v,7} = 5.8$, $\bar{x}_m = 1.2$.

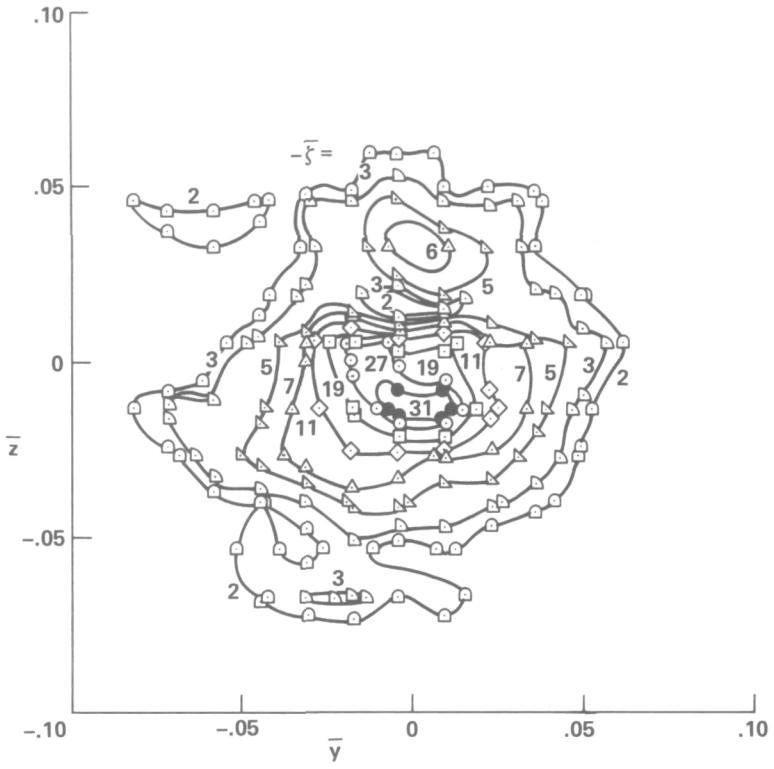

(c) Vorticity.

Figure 10.- Concluded.

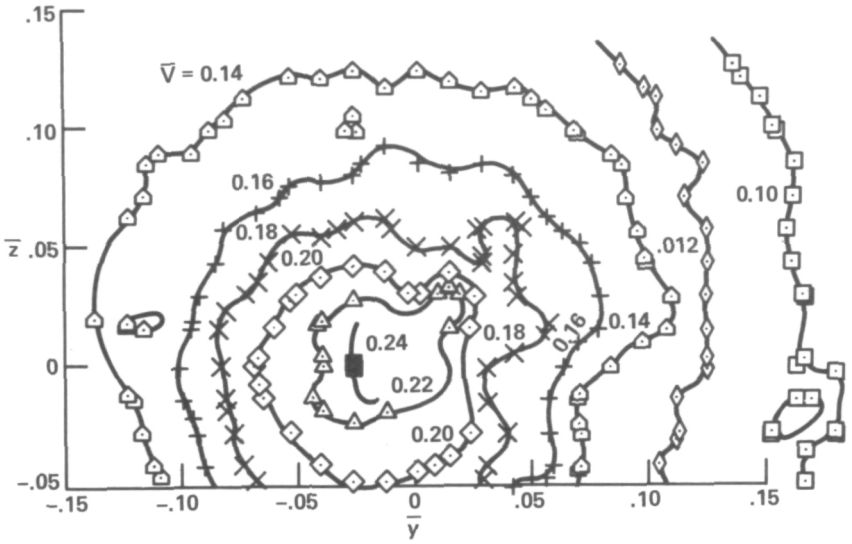

(a) Crossflow velocity.

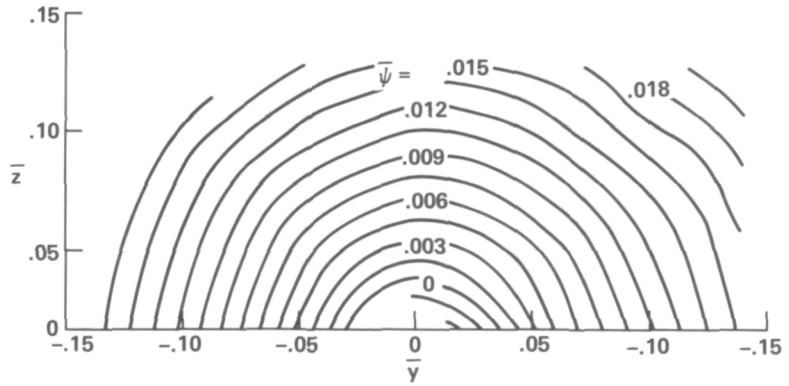

(b) Stream function.

Figure 11.- Results calculated from the measured velocities; b = 724 mm, $\bar{x}_w$ = 7.4, $\bar{x}_m$ = 0.8.

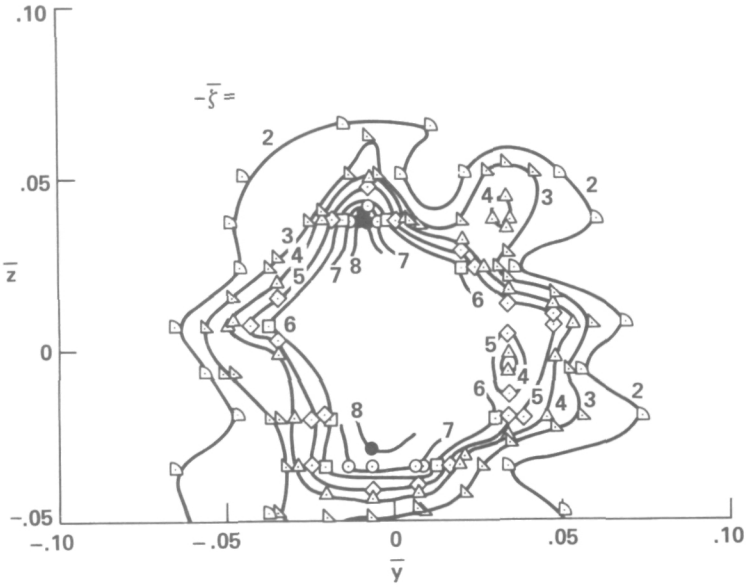

(c) Vorticity.

Figure 11.- Concluded.

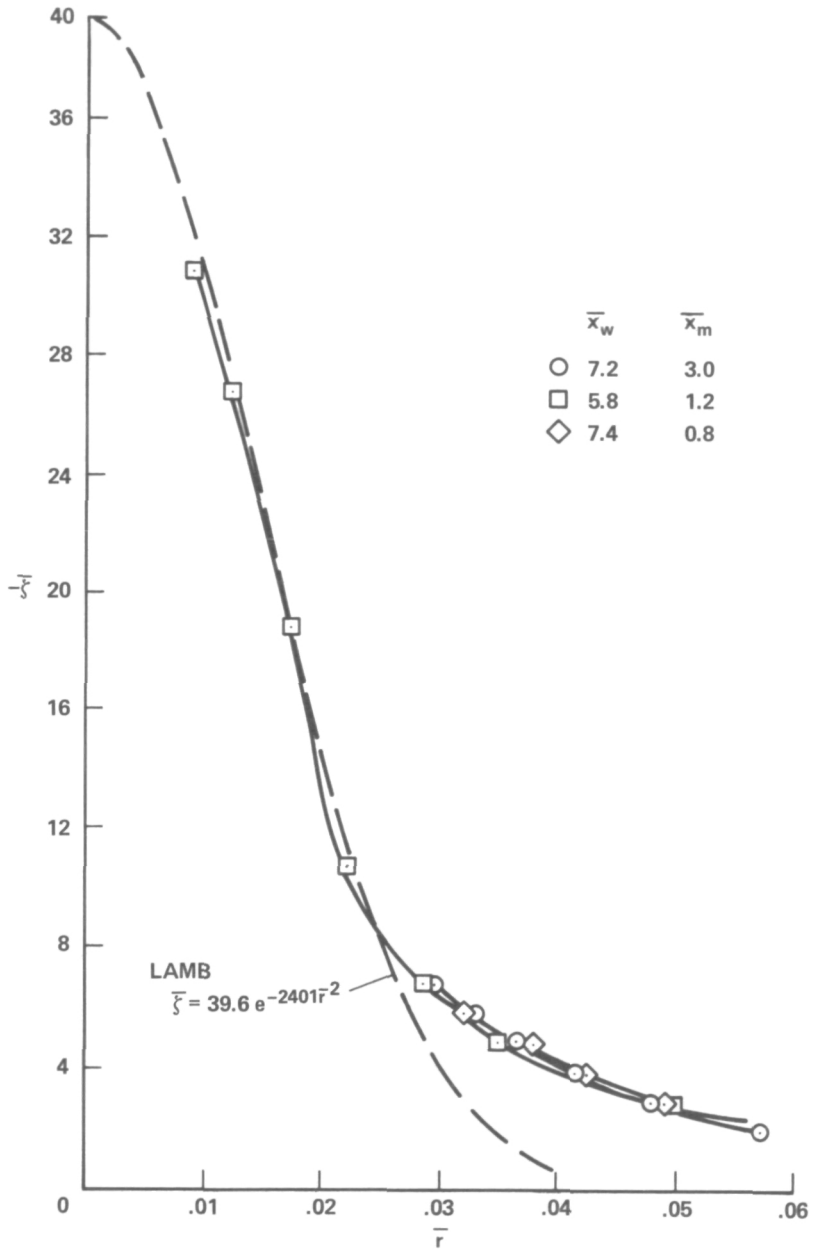

Figure 12.- Variation of vorticity with average radius obtained from contours of vorticity plots. To obtain Lamb profile $\bar{\zeta}$ and $\bar{\Gamma}$ were matched at $\bar{r} = 0.017$.

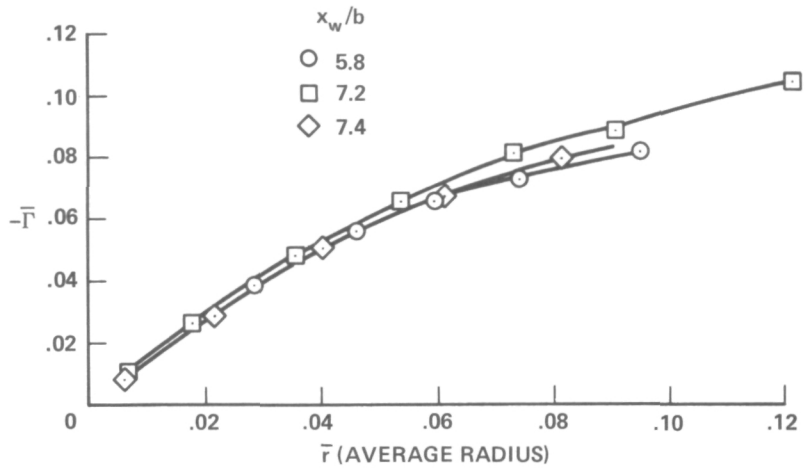

(a) Two wings.

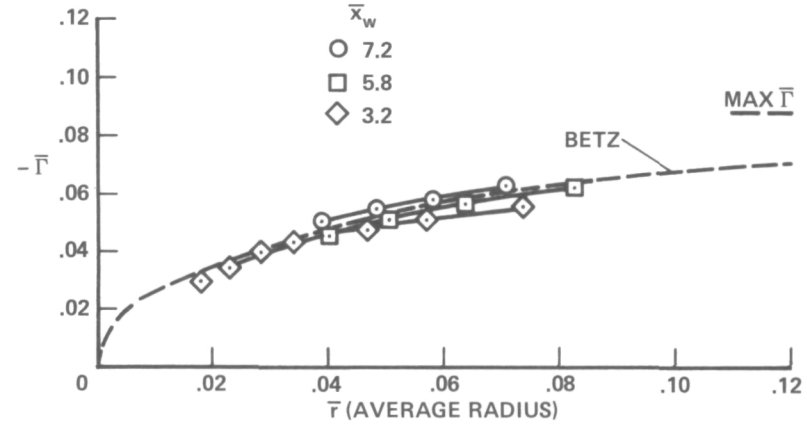

(b) One wing, b = 749 mm.

Figure 13.- Variation of circulation with average radius obtained from contours of circumferential velocity plots (not shown).

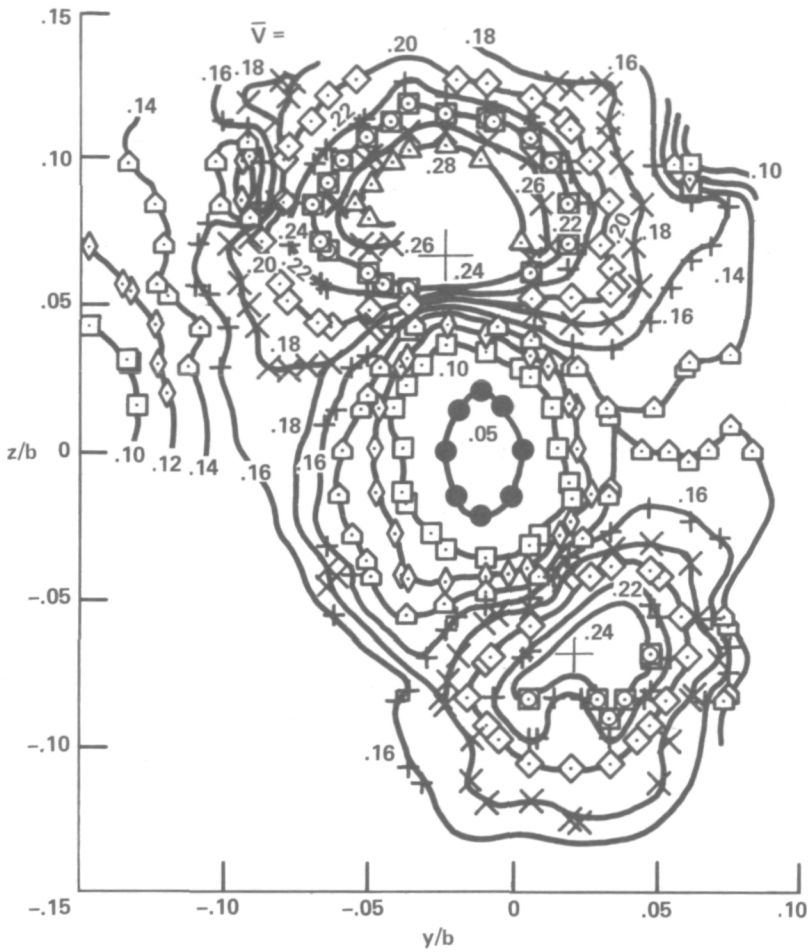

(a) Crossflow velocity.

Figure 14.- Results calculated from the measured velocities at a streamwise station forward of the merger point; b = 724 mm, $\bar{x}_w$ = 1.8, $\bar{x}_m$ = 4.2; "+" indicates flow visualization result for vortex center location.

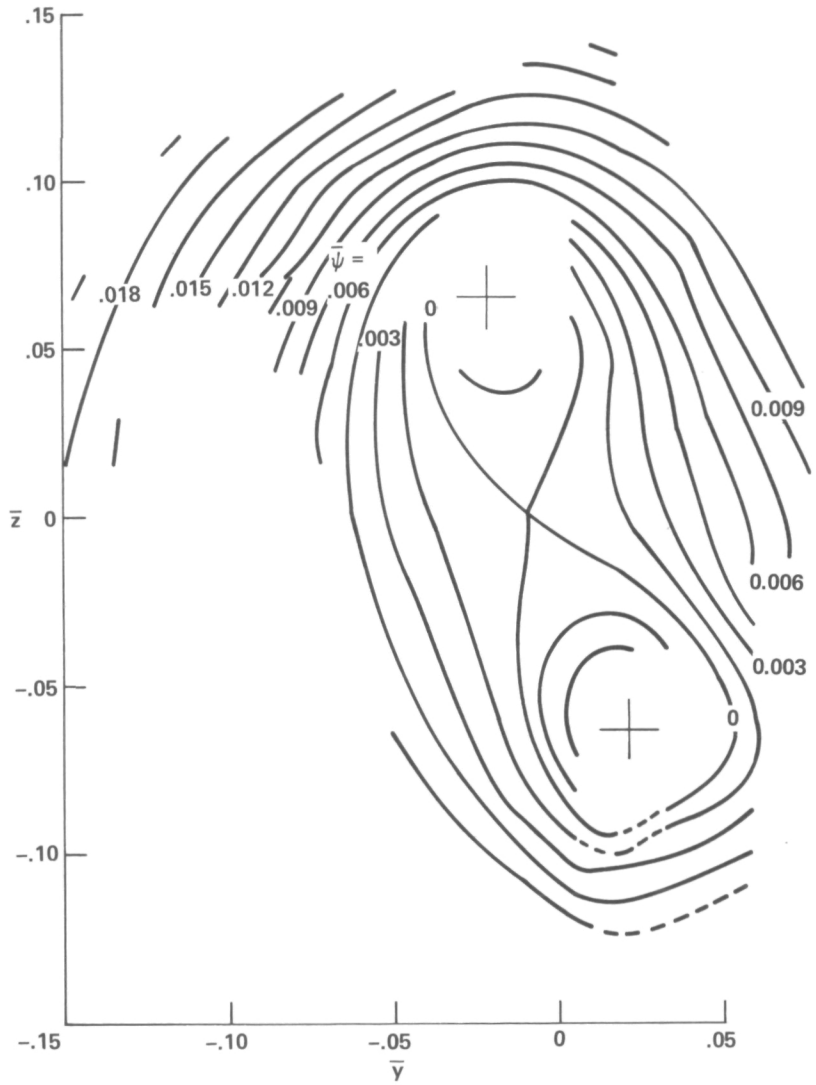

(b) Stream function.

Figure 14.- Continued.

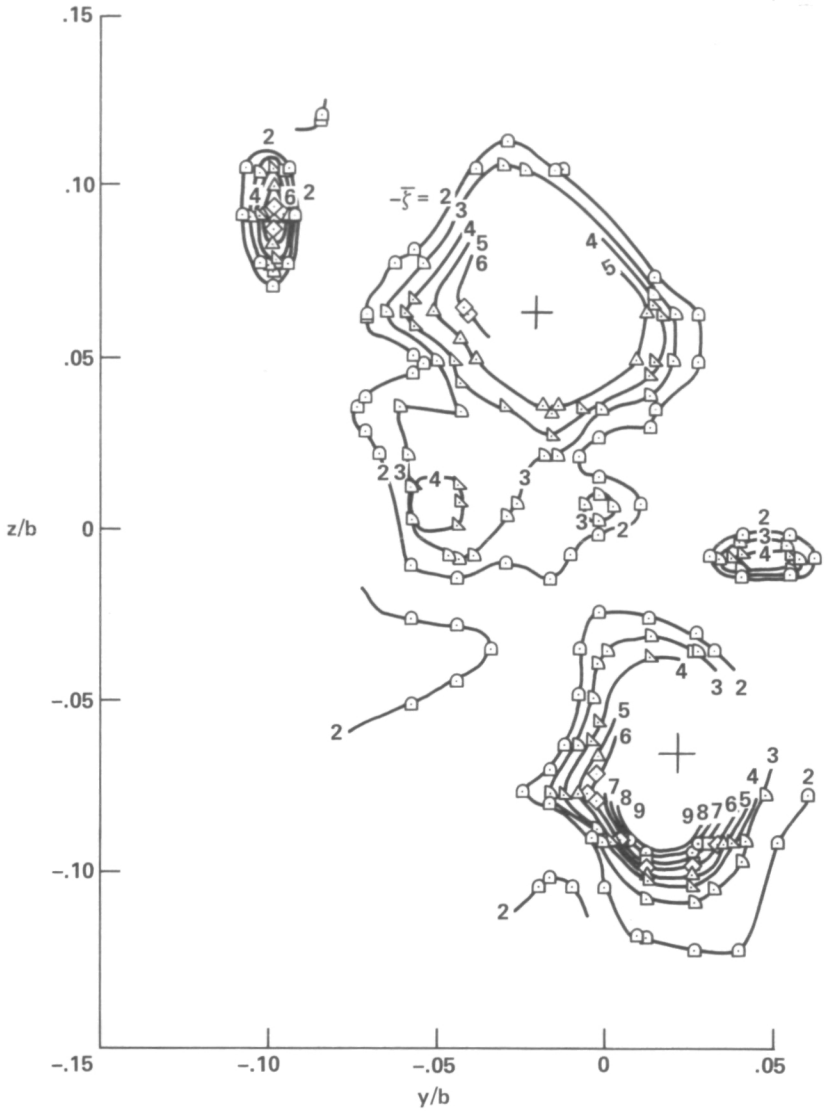

(c) Vorticity.

Figure 14.- Concluded.

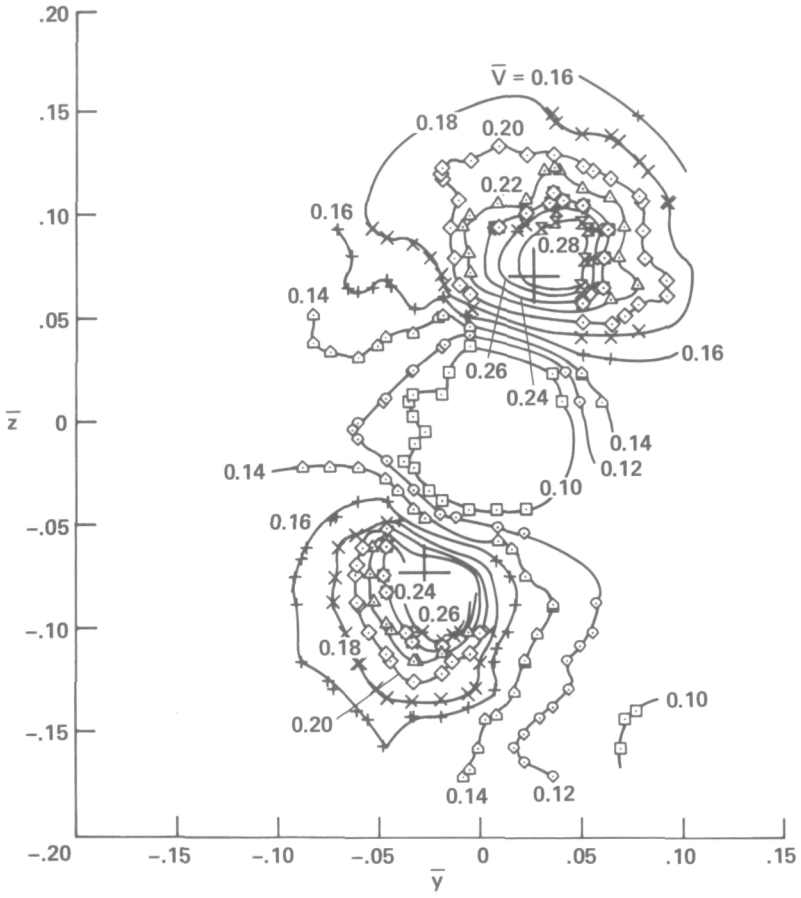

(a) $\bar{V}$, b = 72.4 cm, $\bar{x}_w$ = 3.3

Figure 15.- Contours of velocity magnitude, vorticity, and stream function; 2 wings, α = 10°.

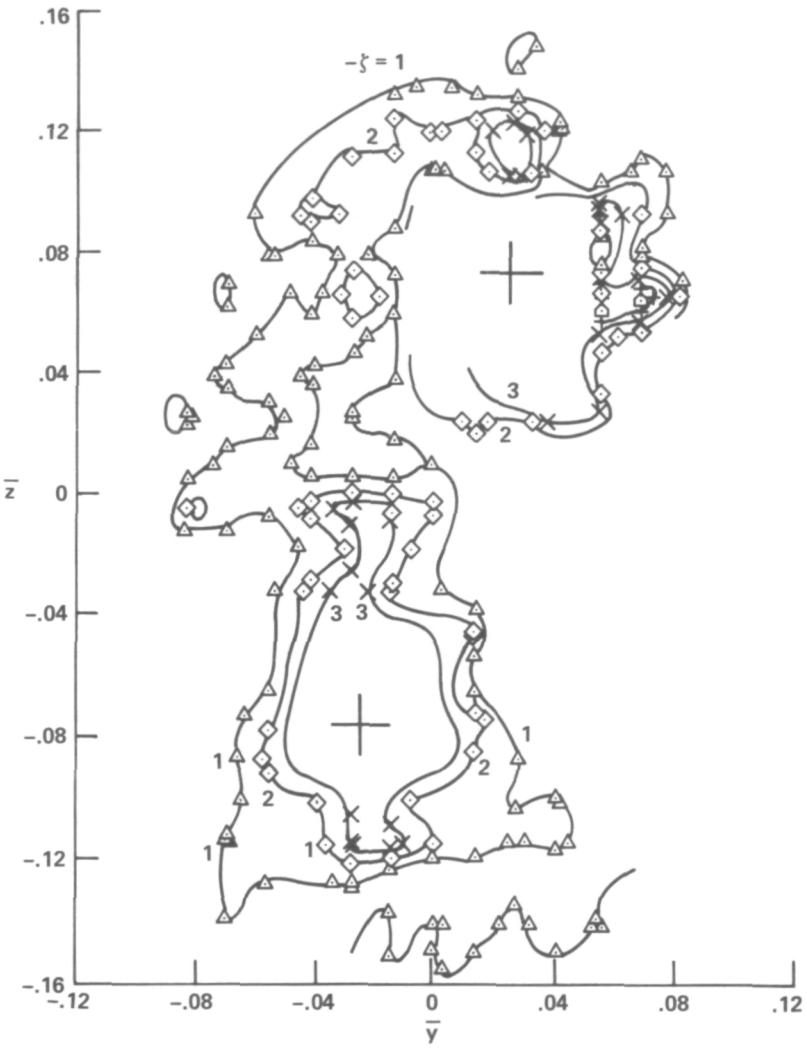

(b) $\bar{\zeta}$, b = 72.4 cm, $\bar{x}_w$ = 3.3

Figure 15.- Continued.

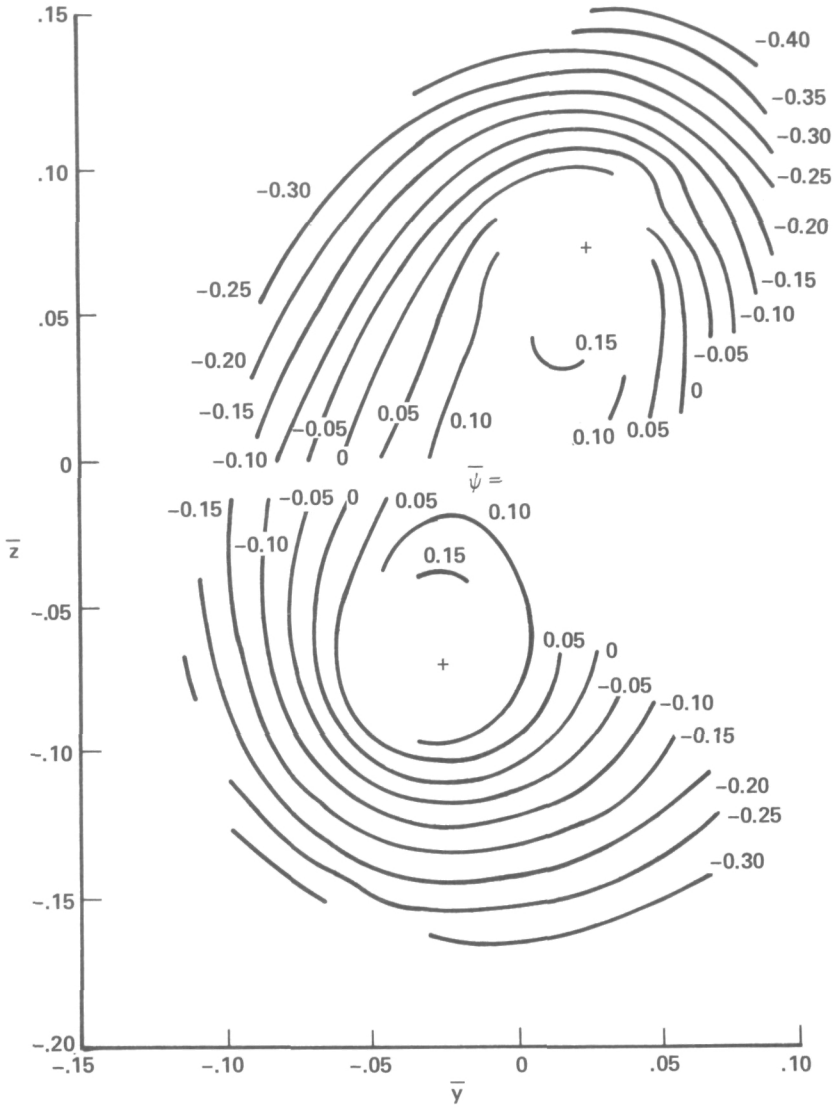

(c) ψ, b = 72.4 cm, $\bar{x}_w$ = 3.3

Figure 15.- Continued.

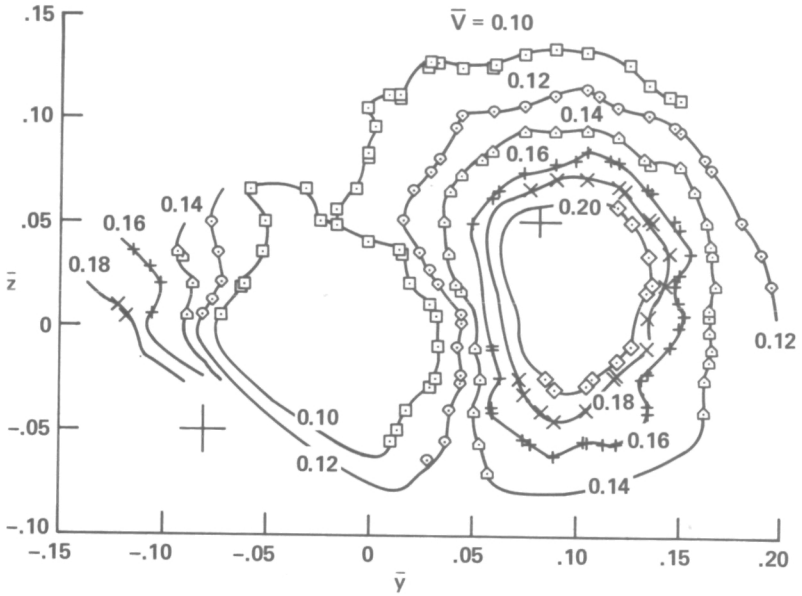

(d) $\bar{V}$, b = 66 cm, $\bar{x}_w$ = 8.2

Figure 15.- Continued.

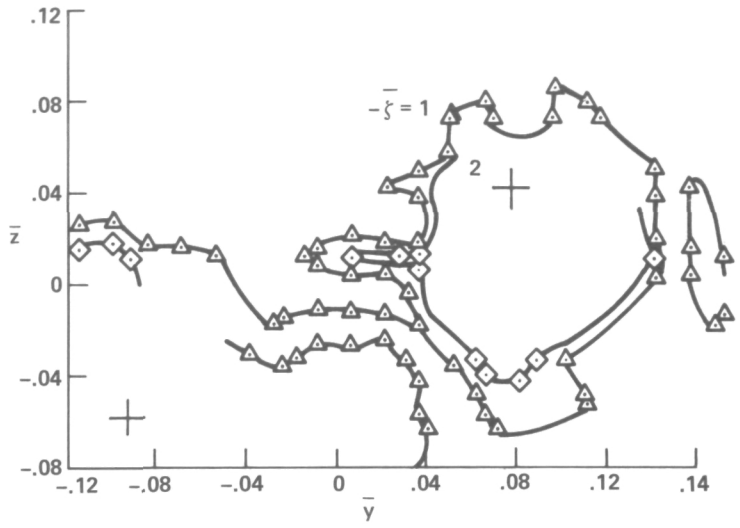

(e) $\bar{\zeta}$, b = 66 cm, $\bar{x}_w$ = 8.2

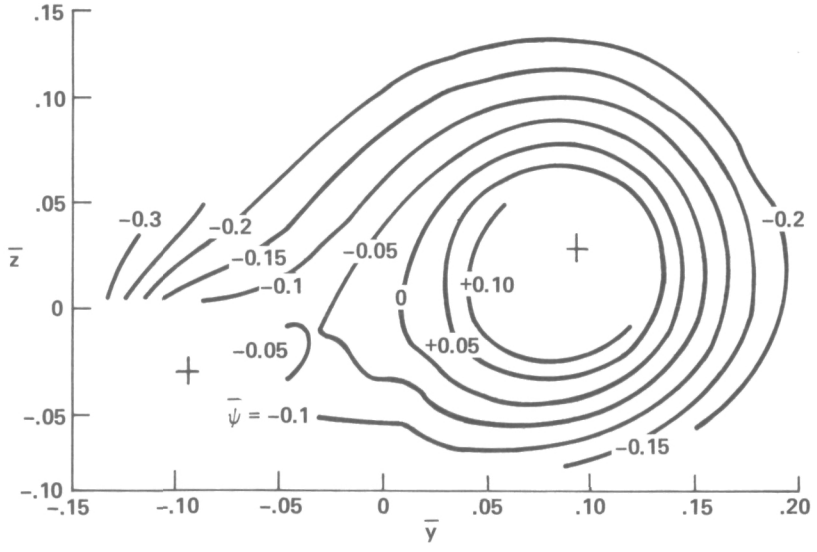

(f) $\bar{\psi}$, b = 66 cm, $\bar{x}_w$ = 8.2

Figure 15.- Concluded.

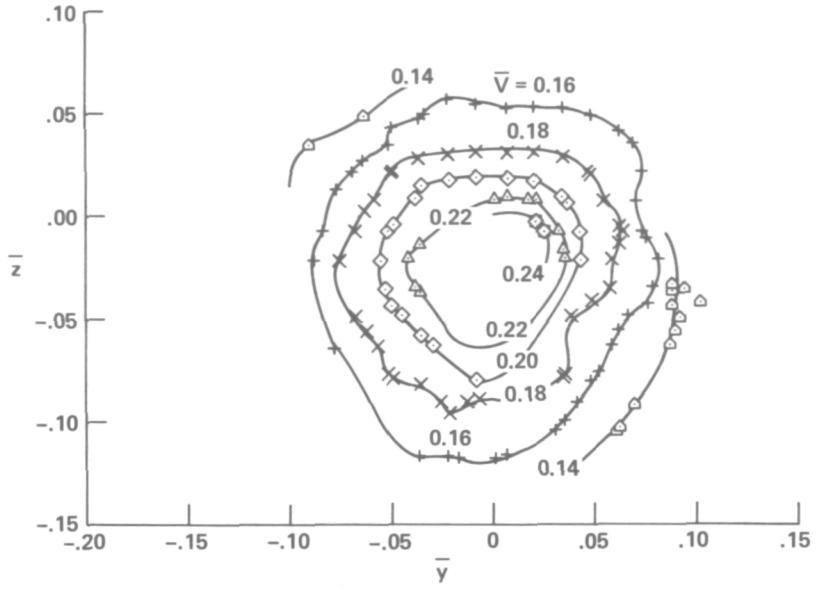

(a) $\bar{V}$, $\bar{x}_w = 7.4$

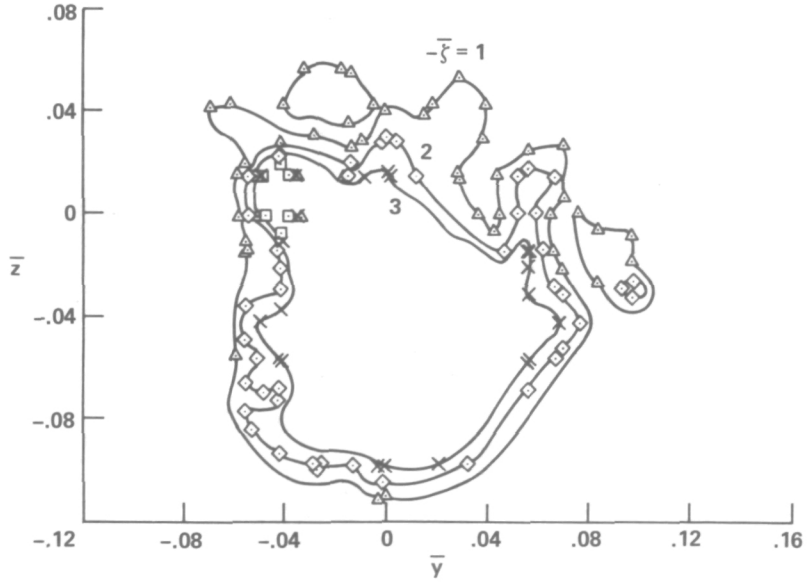

(b) $\bar{\zeta}$, $\bar{x}_w = 7.4$

Figure 16.- Contours of velocity magnitude, vorticity, and stream function with unequal angles of attack; 2 wings, $\alpha_1 = 8°$, $\alpha_2 = 12°$, b = 72.4 cm.

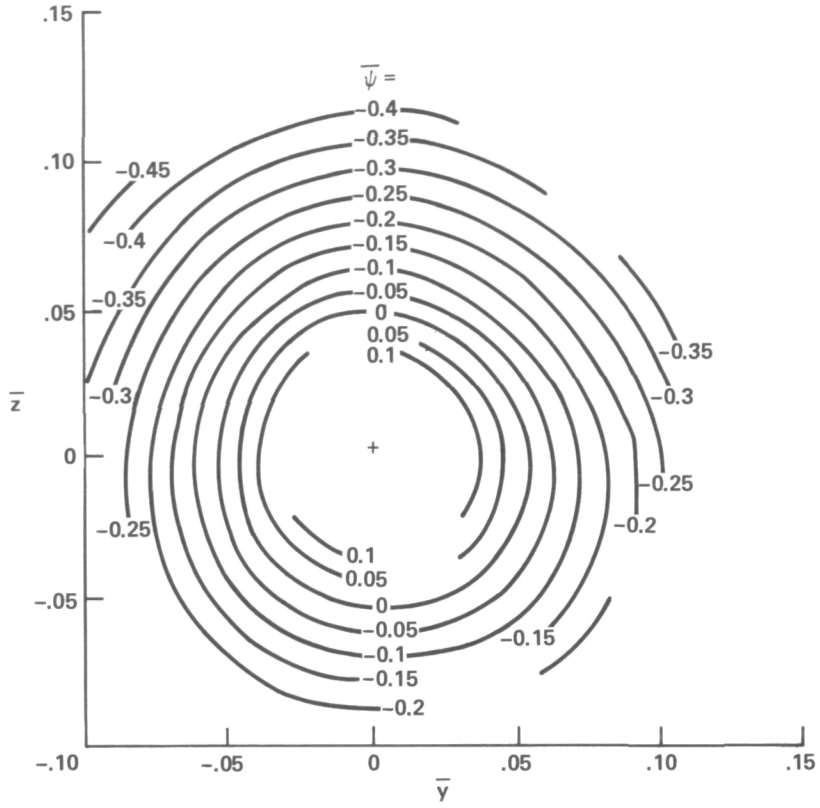

(c) ψ, $\bar{x}_w = 7.4$

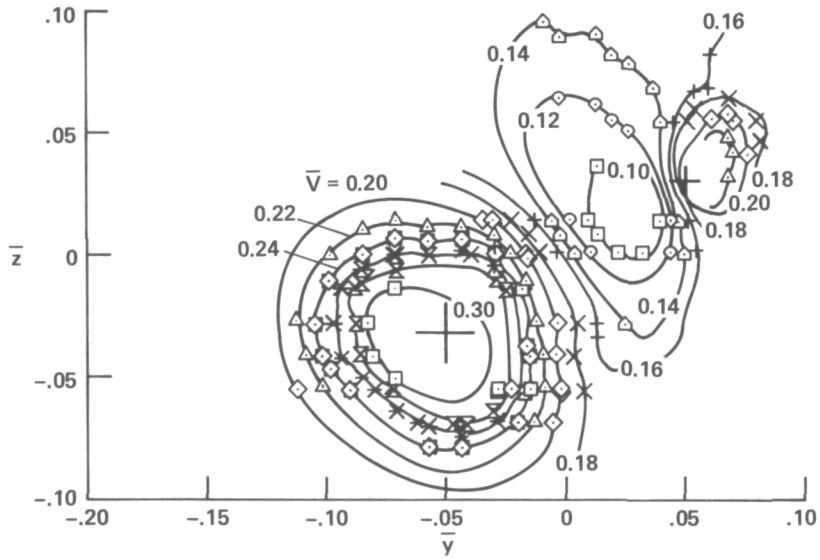

(d) $\bar{V}$, $\bar{x}_w = 3.3$

Figure 16.- Continued.

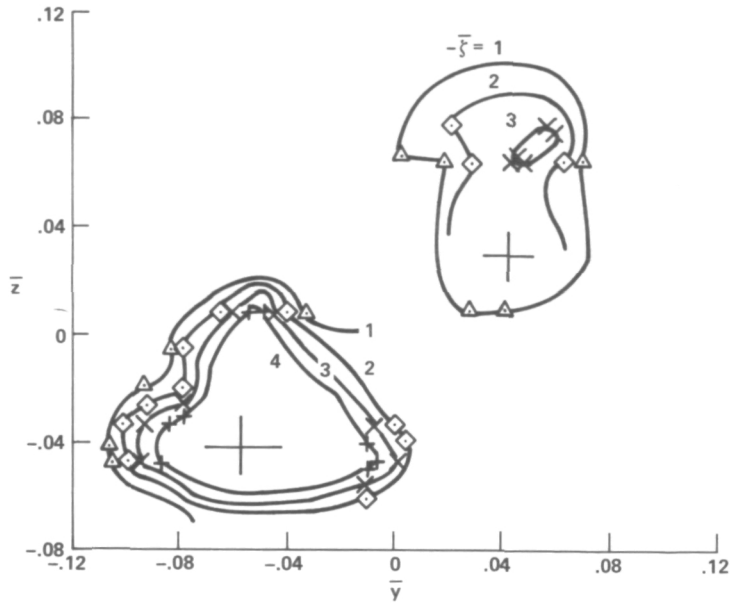

(e) $\bar{\zeta}$, $\bar{x}_w = 3.3$

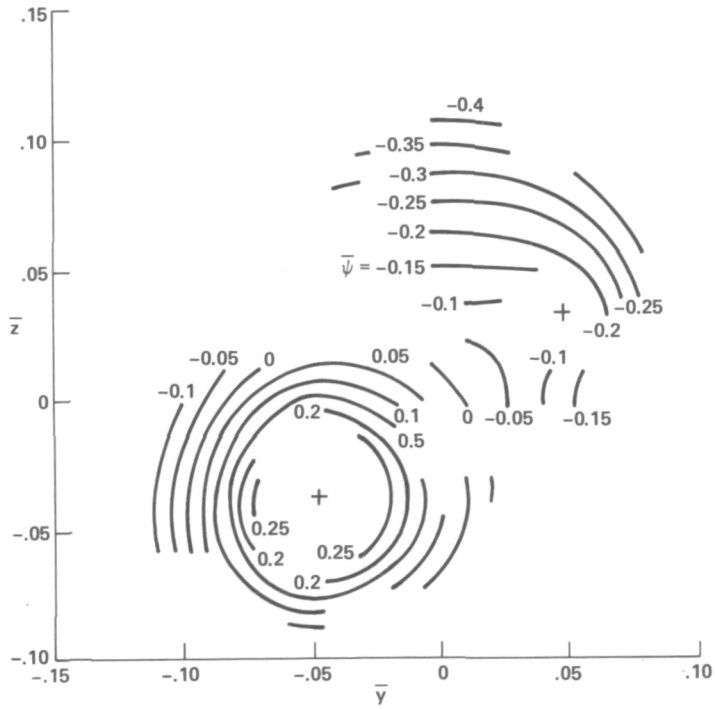

(f) ψ, $\bar{x}_w = 3.3$

Figure 16.- Concluded.

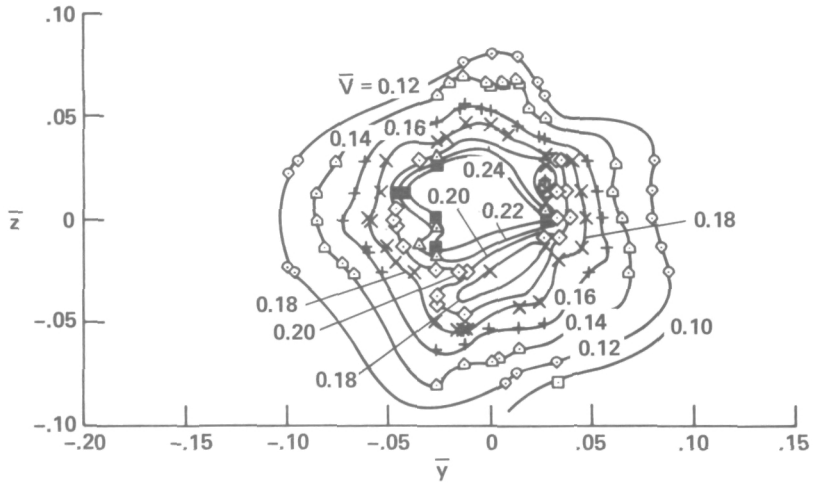

Figure 17.- Contours of velocity magnitude; 1 wing, b = 74.9 cm, $\bar{x}_w$ 7.4, $\alpha = 10°$.

1. Report No.	2. Government Accession No.	3. Recipient's Catalog No.
NASA TM-78449		

4. Title and Subtitle	5. Report Date
LASER-VELOCIMETER SURVEYS OF MERGING VORTICES IN A WIND TUNNEL — COMPLETE DATA AND ANALYSIS	October 1978
	6. Performing Organization Code

7. Author(s)	8. Performing Organization Report No.
Victor R. Corsiglia, James D. Iversen,* and Kenneth L. Orloff	A-7262
	10. Work Unit No. 515-52-10
9. Performing Organization Name and Address	11. Contract or Grant No.
Ames Research Center, NASA Moffett Field, Calif. 94035	
	13. Type of Report and Period Covered
12. Sponsoring Agency Name and Address	Technical Memorandum
National Aeronautics and Space Administration Washington, D.C. 20546	14. Sponsoring Agency Code

15. Supplementary Notes

*Professor, Iowa State University, Ames, Iowa

16. Abstract

The merger of two corotating vortices was studied with a laser velocimeter designed to measure the two cross-stream components of velocity. Measurements were made at several downstream distances in the vortex wake shed by two semispan wings mounted on the wind-tunnel walls. The velocity data provided well-defined contours of crossflow velocity, stream function, and vorticity for a variety of test conditions. Downstream of the merger point, the vorticity was found to be independent of the downstream distance for radii smaller than $r/b = 0.05$. For larger radii, the vorticity depended on the distance from the wing. Upstream of the merger point, a multicell vorticity pattern was found.

17. Key Words (Suggested by Author(s))	18. Distribution Statement
Wind tunnel Vortices Laser velocimeter	Unlimited STAR Category - 02

19. Security Classif. (of this report)	20. Security Classif. (of this page)	21. No. of Pages	22. Price*
Unclassified	Unclassified	48	$4.00

*For sale by the National Technical Information Service, Springfield, Virginia 22161

NASA-Langley, 1978

National Aeronautics and
Space Administration

Washington, D.C.
20546

Official Business
Penalty for Private Use, $300

THIRD-CLASS BULK RATE

Postage and Fees Paid
National Aeronautics and
Space Administration
NASA-451

U.S.MAIL

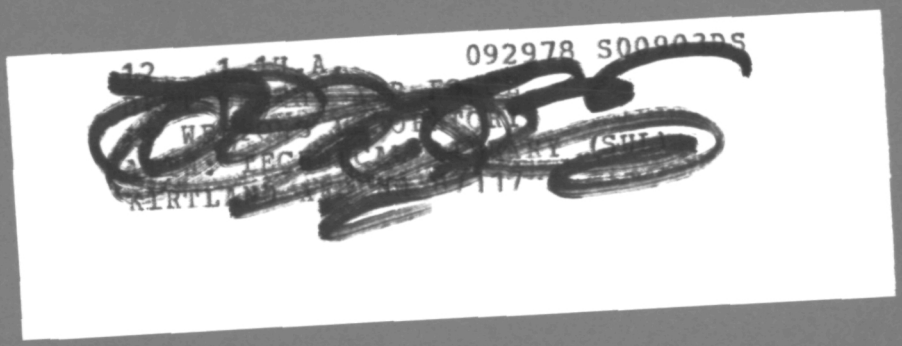

NASA

POSTMASTER: *If Undeliverable (Section 158 Postal Manual) Do Not Return*